ADDIS ABABA UNIVERSITY

SCHOOL OF GRADUATE STUDIES

FACULTY OF TECHNOLOGY

"Modeling Static and Dynamic of Milling Machine End Mill and Tool Holder"

A Thesis Submitted to the Faculty of Technology, Department of Mechanical Engineering, in partial fulfillment for the Degree of Master of Science in Mechanical Design Engineering

By

Shimels Eshete Wale

Advisor

Dr.-ing.Tamrat Tesfaye

Addis Ababa Ethiopia

March 2010

ADDIS ABABA UNIVERSITY SCHOOL OF GRADUATE STUDIES

FACULTY OF TECHNOLOGY

"Modeling Static And Dynamic Of Milling Machine End Mill And Tool Holder"

By

Shimels Eshete wale

Approval by Board of examiners:

Dr.-ing. Edessa Dribssa Chairman	---------- Signature
Department of Mechanical Eng'g	
Dr. -ing. Tamrat Tesfaye	----------
(Advisor)	Signature
Dr. Abiy Awoke	----------
External Examiner	Signature
Prof. Idalberto	----------
Internal Examiner	Signature

ABSTRACT

An end mill is a tool used on a milling machine. A milling machine is a machine found in a metal working shop that is used to remove material from a metal block to make it into a finished part. And it is one of the tools used on the milling machine to make a particular type of cut. Productivity and surface quality in milling processes have direct effects on cost, production lead time and quality of machined parts.

Chatter vibrations in milling, which develop due to dynamic interactions between the cutting tool and the workpiece, result in reduced productivity and part quality. Machine tool chatter causes machining instability, surface roughness, and tool wear in metal cutting processes. The excessive vibrations of the cutter and workpiece result in poor surface finish, dimensional accuracy and may damage the workpiece and machine tool. In addition to this cutting force produce deformations of the tool and this cause dimensional and form errors on the workpiece.

In this research, generalized equations are presented which can be used for predicting static and dynamic properties of the cutting tool. Milling forces are modeled for given cutter geometry, cutting conditions and work material. The static and dynamic characteristics of tool and tool holder can be obtained by using finite element analysis (FEA); simplified equations are created to predict deflections of tools for given geometric parameters and material properties and also for natural frequencies and mode shapes of cutter dynamics. Finite Element Analysis (FEA) results are compared with the results obtained from analytic equations, Comparison of natural frequencies between carbide and HSS end mills. And a simple method to analytically calculate the approximate optimum depths of cut and determine the corresponding spindle speeds by creating the stability lobe diagram. Chatter vibration free spindle speeds and axial depth of cuts can be selected from stability chats. The characteristics and limitations of the stability lobe diagram are discussed. Case studies are also provided to illustrate the method and verify the results.

ACKNOWLEDGEMENTS

A long journey has come to an end and I wish to thank all the people who crossed my path of life, who influenced me in ways I realized and in ways I did not and this work would not have been possible without the support, guidance, and encouragement of many individuals friends, colleagues and parents, over the past many years. I take this opportunity to express my gratitude to them in a very small way.

I have been very lucky to have had Dr.ing TAMRAT TESFAYE my M.Sc advisor. I would like to express my sincere gratitude to him for giving me the opportunity to work with him. I have benefited enormously from his approach to problem solving and his exciting teaching. The interesting discussions with him and his critical comments have shaped my thinking to a large extent.

My greatest thankfulness to Ato YOHANIS LIKU and W/T FASIKA ESHETE, who have always been there to support and encourage me and the decisions I have made, throughout my life. Their constant love and limitless support, encouragement, and advice had a great part in bringing me into the person I am today.

Last, I owe great thanks to my family for there love, encouragement, and being my company for countless good or bad days.

TABLE OF CONTENT

List of Tables

List of Figures

CHAPTER ONE

INTRODUCTION AND BACKGROUND

1.1 Introduction

Milling is one of the most commonly used machining processes in industry. Great variety of parts with different geometry, complexity, quality and materials can be produced by milling. In milling the main cutting motion is the rotation of a multitoothed cutter that machines a workpiece that performs translative feed motions. There are two basic models, face milling and peripheral milling (up and down milling). A very common type of peripheral milling is end milling (Figure 1.1). The geometry of end milling operation is presented in Figure 1.2.

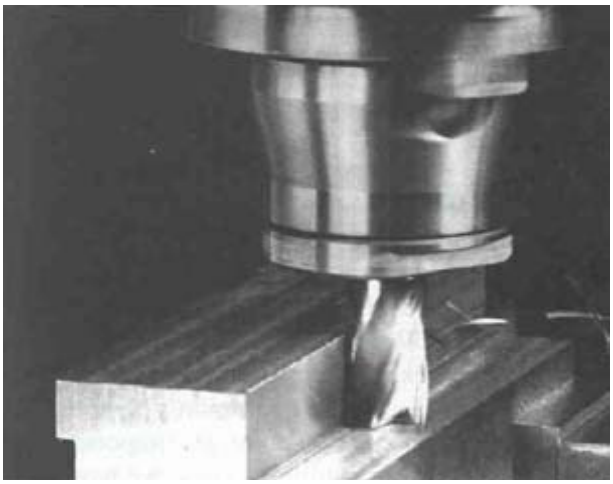

Figure 1.1: End milling operation

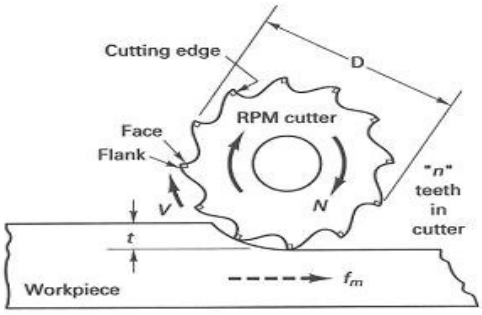

Figure 1.2: Geometry of end milling

Depending on the workpiece geometry, different milling cutters are used. And Tool holders are used to provide good concentricity between tool and machine spindle. (Figure 1.3)

Figure 1.3: Various milling cutting tools and tool holders

An end mill is a cutter of a smaller diameter (usually between 5 mm and 30 mm diameter) clamped in overhang, and its length is several times its diameter. Figure 1.4 shows an end mill with detail geometric properties.

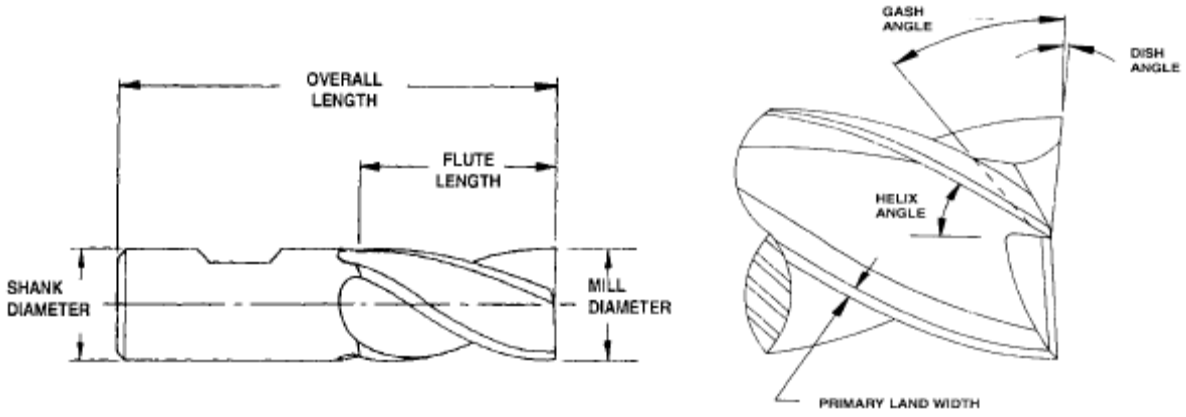

Figure 1.4: Geometric properties of the end mill

Static and dynamic deformations of cutting tool play an important role in tolerance integrity and stability in a machining process affecting part quality and productivity. Modeling is needed for prediction static and dynamic properties of cutting tool without measurement. The models can be integrated into CAD/CAM systems in order to achieve a virtual machining system where most of the effects that are observed in real machining could be simulated in advance.

1.2 Objective of the project

The objective of this thesis is to increase productivity and quality in milling operations by reducing high cutting forces and controlling chatter vibrations. This will be done through the following work:

- Simplified equations are created to predict deflections of tools for given geometric parameters and material properties in static analysis and to calculate the natural frequencies and mode shapes of segmented beam geometries in the cutting tool dynamics. Both FEA and analytical methods will have used for static and dynamic analysis of end mills.

- Creating a stability lobe diagram based on regenerative chatter theory which is an effective tool to predict and control chatter. This method allows machine operators to practically choose cutting parameters, instructors to effective teach the regenerative chatter theory, and students to easily create stability lobe diagrams and practice optimizing cutting parameters.

1.3 Scope and Limitation of the Study

The aim of this thesis is to avoid unstable forced vibration of the cutting tool during a machining process which is called chatter and to improve productivity and quality of the products using modeling and simplified equations with finite element method package ANSYS software due its availability.

The scope of this thesis is limited to studying milling process models, deflection and surface generation model, explanation of geometric properties and material characteristics of tool and tool holder, models for end mill static deformations, development of generalized equations, the static characteristics of tool and tool holder are obtained using FEA analysis, a method of modeling for transverse vibrations of geometrically segmented beam, Finite Element Analysis (FEA) results of various tool geometries, different materials and tool holder types are given. These results are compared with the results obtained from analytic equations and finally creating of stability diagram.

1.4 Methodology of the study

End milling is a commonly used process in industry for parts with dimensional and surface quality requirements. Chapter 3 gives process models [Budak, E., 2002] that can be used improve productivity and quality. An analytical milling force model, which is used tool deflection calculations, is prediction presented. The prediction of form error is demonstrated. An analytical model for of chatter stability limit is presented.

Chapter 4 gives simplified equations to predict maximum tool deflection. Because of the complex end mill geometry beam approximations do not provide accurate stiffness and transfer function predictions. The moment of inertias of different end mill cross sections must be determined [Nermes et al., 2001]. In static analysis, moment area method [Beer and Johnson, 1992] is used to calculate the deflection of end mill, which have two segments, one for part with flute and the other for the shank. ANSYS finite element analysis results for tool and tool holder is also presented in this chapter Analytical equation solutions are compared with FEA results.

Chapter 5 starts with a brief explanation segmented beam model that is used to predict tool dynamics. The solution of mode shapes and fundamental natural frequency is presented [Rao, 1995]. In order to avoid complex calculations simplified equations are determined finite element dynamic analysis results for tool and tool holder are given. Transfer function measurement system and modal analysis are described.

Chapter 6 we have discussed the fundamental concepts and procedures in creating a stability lobe diagram and a method of using a spreadsheet to create stability lobe diagrams is presented.

A conclusion of the study is provided in Chapter 7 summarizing the results achieved.

1.5 Background

Milling is one of the most commonly used machining processes in industry. Great variety of parts with different geometry, complexity, quality and materials can be produced by milling. In milling the main cutting motion is the rotation of a multitoothed cutter that machines a workpiece that performs translative feed motions. The cutting action of the many teeth around the milling cutter provides a fast method of machining. The machined surface may be flat, angular, or curved. The surface may also be milled to any combination of shapes. The machine for holding the workpiece, rotating the cutter, and feeding it is known as the Milling Machine [2].

1.5.1 **Types of Milling Machine**

Most of the milling machines are constructed of column and knee structure and they are classified into two main types namely Horizontal Milling Machine and Vertical Milling Machine. The name Horizontal or Vertical is given to the machine by virtue of its spindle axis. Horizontal machines can be further classified into Plain Horizontal and Universal Milling Machine. The main difference between the two is that the table of a Universal Milling Machine can be set at an angle for helical milling while the table of a Plain Horizontal Milling Machine is not [Efunda, 2000].

1.5.2 Horizontal Milling Machine

Figure 2.1 shows the main features of a Plain Horizontal Milling Machine.

Their functions are:-

a. Column: - The column houses the spindle, the bearings, the gear box, the clutches, the shafts, the pumps, and the shifting mechanisms for transmitting power from the electric motor to the spindle at a selected speed.

b. Knee: - The knee mounted in front of the column is for supporting the table and to provide an up or down motion along the Z axis.

c. Saddle: - The saddle consists of two slideways, one on the top and one at the bottom located at 90º to each other, for providing motions in the X or Y axes by means of lead screws.

d. Table: - The table is mounted on top of the saddle and can be moved along the X axis. On top of the table are some T-slots for the mounting of workpiece or clamping fixtures.

e. Arbor: - The arbor is an extension of the spindle for mounting cutters. Usually, the thread end of an arbor is of left hand helix.

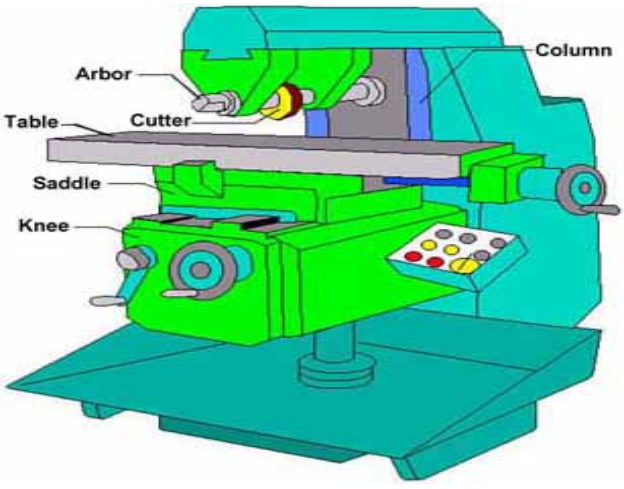

Figure 1.5:-Horizontal Milling Machine

1.5.3 Vertical Milling Machine

Figure 2.2 shows a vertical milling machine which is of similar construction to a horizontal milling machine except that the spindle is mounted in the vertical position.

Its additional features are: -

a. Milling head: - The milling head consisting the spindle, the motor, and the feed control unit is mounted on a swivel base such that it can be set at any angle to the table.

b. Ram: - The ram on which the milling head is attached can be positioned forward and backward along the slideway on the top of the column.

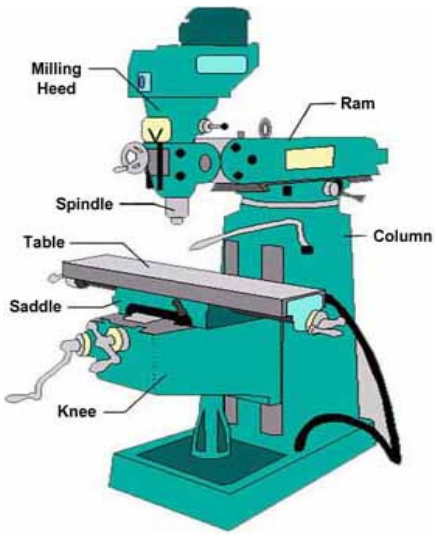

Figure 1.6:- Vertical Milling Machine

1.6 Milling Cutters

A milling cutter is a cutting tool that is used on a milling machine. Milling cutters are available in many standard and special types, forms, diameters, and widths. The teeth may be straight (parallel to the axis of rotation) or at a helix angle. The helix angle helps a slow engagement of the tool distributing the forces .The cutter may be right-hand (to turn clockwise) or left-hand (to turn counterclockwise).The figure shows a typical end milling cutter.

1.6.1 Features of Milling Cutters

Some of the terms used to identify the major features of a milling cutter are given in the figure.1.7

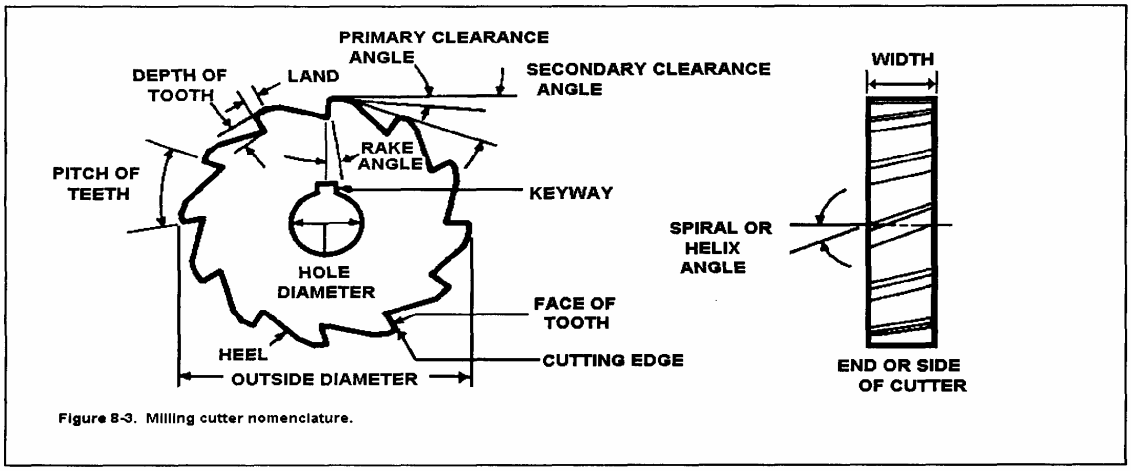

Figure 1.7:-Features of milling cutters

1.6.2 Cutting Tools and Tool Holders

Depending on the workpiece geometry, different milling cutters are used. And also different tool holders are used to provide good concentricity between tool and machine spindle. (Figure1.8)

1.6.3 Types of Milling Cutters

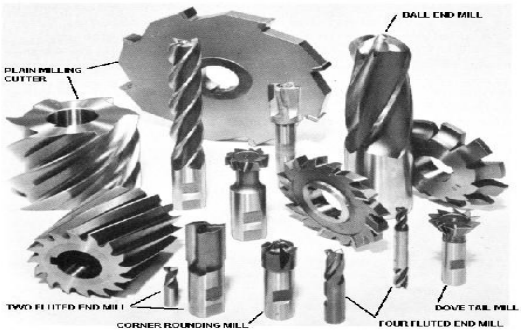

Figure 1.8:- Various milling cutting tools and tool holders

1.6.3.1 Cutting tools for Vertical Milling

a.End Mills

Commonly used for facing, slotting and profile milling.

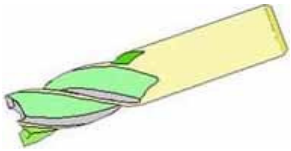

Figure 1.9 End Mill

b. Rough Cut End Mills

For rapid metal removal.

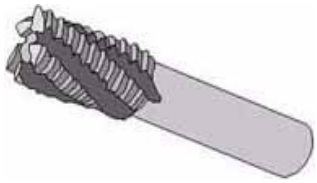

Figure1.10 Rough Cut End Mill

c.Slot Drills

For producing pockets without drilling a hole before hand.

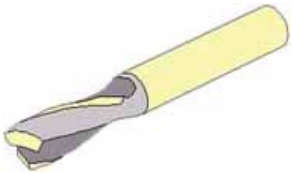

Figure1.11 Slot Drill

d.Face Milling Cutters

For heavy cutting.

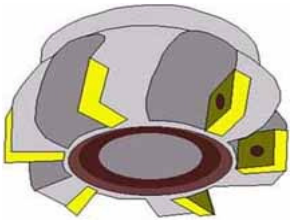

Figure 1.12 Face Milling Cutter

Most vertical milling cutters are of end mill types and are specified by the material, the diameter, the length, the helical angle, the types of shank and the shank diameter. For face milling cutter, only the diameter of the cutter and the types of carbide inserts are required.

1.7 **Milling Processes**

Milling is a metal removal process by means of using a rotating cutter having one or more cutting teeth as illustrated in figure 2.12.

Cutting action is carried out by feeding the workpiece against the rotating cutter. Thus, the spindle speed, the table feed, the depth of cut, and the rotating direction of the cutter become the main parameters of the process. Good results can only be achieved with well balanced settings of these parameters.

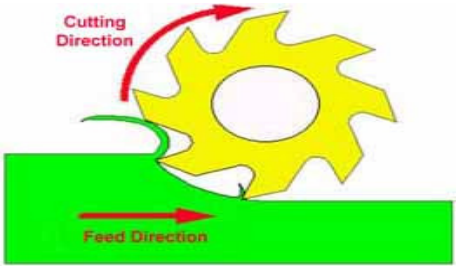

Figure 1.13 Milling Process with geometry of end milling

a. Spindle Speed

$$N = \frac{CS \times 1000}{\pi d}$$

Spindle speed in revolution per minute (R.P.M.) for the cutter can be calculated from the equation: -where – N = R.P.M. of the cutter

CS = Linear Cutting Speed of the material in m/min. (see table 1)

d = Diameter of cutter in mm

b. Feed Rate: -Feed rate (F) is defined as the rate of travel of the workpiece in mm/min. But most tool suppliers recommend it as the movement per tooth of the cutter (f). Thus,

$$F = f .u. N$$

where – F = table feed in mm/min

f = movement per tooth of cutter in mm (see table 1)

u = number of teeth of cutter

N = R.P.M. of the cutter

where C.S. and feed rate for some common material:-

Tool Material	High Speed Steel		Carbide	
Material	Cutting Speed	Feed(f)	Cutting Speed	Feed(f)
Mild Steel	25	0.08	100	0.15
Aluminum	100	0.15	500	0.3
Hardened Steel	---	---	50	0.1

Table 1.1:- C.S. and feed rate for some common material

1.7.1 Depth of Cut

Depth of cut is directly related to the efficiency of the cutting process. The deeper the cut the faster will be the production rate. Yet, it still depends on the strength of the cutter and the material to be cut.

For a certain type of cutter, a typical range of cut will be recommended by the supplier. Nevertheless, it should be noted that a finer cut is usually associated with a better surface finish as well as a long tool life.

1.7.2 Direction of Cutter Rotation

a. Up Cut Milling

In up cut milling, the cutter rotates in a direction opposite to the table feed as illustrated in figure 2.13. It is conventionally used in most milling operations because the backlash between the leadscrew and the nut of the machine table can be eliminated.

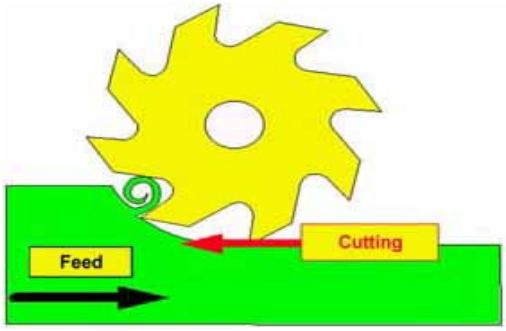

Figure 1.14 Up Cut Milling

b. **Down Cut Milling**

In down cut milling, the cutter rotates in the same direction as the table feed as illustrated in figure 2.14. This method is also known as Climb Milling and can only be used on machines equipped with a backlash eliminator or on a CNC milling machine. This method, when properly treated, will require less power in feeding the table and give a better surface finish on the workpiece.

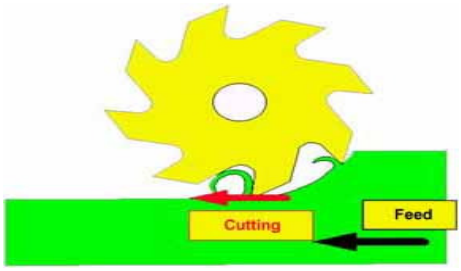

Figure1.15 Down Cut Milling

1.7.3 Classification of Milling

 Peripheral Milling

In peripheral (or slab) milling, the milled surface is generated by teeth located on the periphery of the cutter body. The axis of cutter rotation is generally in a plane parallel to the workpiece surface to be machined**.**

 Face Milling

In face milling, the cutter is mounted on a spindle having an axis of rotation perpendicular to the workpiece surface. The milled surface results from the action of cutting edges located on the periphery and face of the cutter.

 End Milling

The cutter in end milling generally rotates on an axis vertical to the workpiece. It can be tilted to machine tapered surfaces. Cutting teeth are located on both the end face of the cutter and the periphery of the cutter body.

.The chip formation in down milling is opposite to the chip formation in up milling. The figure for down milling shows that the cutter tooth is almost parallel to the top surface of the workpiece. The cutter tooth begins to mill the full chip thickness. Then the chip thickness gradually decreases.

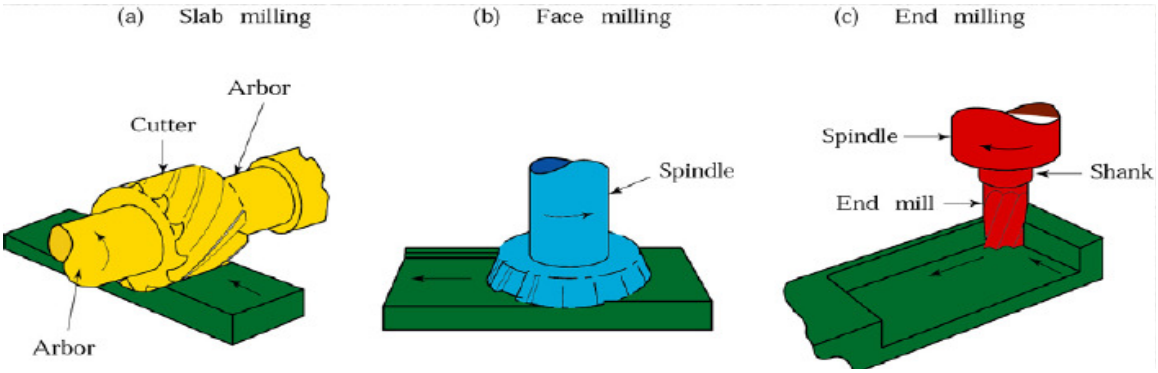

Figure 1.16 some of the basic types of milling cutters and milling operations.

1.7.4 Features of a Milling Cutter

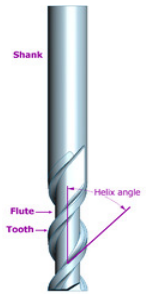

Figure1.17:- An End Mill cutter with two flutes

Milling cutters come in several shapes and many sizes. There is also a choice of coatings, as well as rake angle and number of cutting surfaces.

Shape**: -** Several standard shapes of milling cutter are used in industry today, which are explained in more detail below.

Flutes / teeth: - The flutes of the milling bit are the deep helical grooves running up the cutter, while the sharp blade along the edge of the flute is known as the tooth. The tooth cuts the material, and chips of this material are pulled up the flute by the rotation of the cutter. There is almost always one tooth per flute, but some cutters have two teeth per flute. Often, the words flute and tooth are used interchangeably. Milling cutters may have from one to many teeth, with 2, 3 and 4 being most common. Typically, the more teeth a cutter has, the more rapidly it can remove material. So, a 4-tooth cutter can remove material at twice the rate of a 2-tooth cutter.

Helix angle: - The flutes of a milling cutter are almost always helical. If the flutes were straight, the whole tooth would impact the material at once, causing vibration and reducing accuracy and surface quality. Setting the flutes at an angle allows the tooth to enter the material gradually, reducing vibration. Typically, finishing cutters have a higher rake angle (tighter helix) to give a better finish.

Center cutting: - Some milling cutters can drill straight down (plunge) through the material, while others cannot. This is because the teeth of some cutters do not go all the way to the centre of the end face. However, these cutters can cut downwards at an angle of 45 degrees or so.

Roughing or Finishing: - Different types of cutter are available for cutting away large amounts of material, leaving a poor surface finish (roughing), or removing a smaller amount of material, but leaving a good surface finish (finishing). A roughing cutter may have serrated teeth for breaking the chips of material into smaller pieces. These teeth leave a rough surface behind. A finishing cutter may have a large number (4 or more) teeth for removing material carefully. However, the large number of flutes leaves little room for efficient swarf removal, so they are less good for removing large amounts of material.

Coatings: - The right tool coatings can have a great influence on the cutting process by increasing cutting speed and tool life, and improving the surface finish. Polycrystalline Diamond (PCD) is an exceptionally hard coating used on cutters which must withstand high abrasive wear. A PCD coated tool may last up to 100 times longer than an uncoated tool. However the coating cannot be used at temperatures above 600 degrees C, or on ferrous metals. Tools for machining aluminium are sometimes given a coating of TiAlN. Aluminium is a relatively sticky metal, and can weld itself to the teeth of tools, causing them to appear blunt. However it tends not to stick to TiAlN, allowing the tool to be used for much longer in aluminium.

Shank: - The shank is the cylindrical (non-fluted) part of the tool which is used to hold and locate it in the tool holder. A shank may be perfectly round, and held by friction, or it may have a Weldon Flat, where a grub screw makes contact for increased torque without the tool slipping. The diameter may be different from the diameter of the cutting part of the tool, so that it can be held by a standard tool holder.

1.7.5 Using a Milling Cutter

1.7.5.1 Chip Formation

Although there are many different types of milling cutter, understanding chip formation is fundamental to the use of any of them. As the milling cutter rotates, the material to be cut is fed into it, and each tooth of the cutter cuts away small chip of material [4]. Achieving the correct size of chip is of critical importance. The size of this chip depends on several variables.

- Surface cutting speed (V_c): This is the speed at which each tooth cuts through the material as the tool spins. This is measured either in meters per minute in metric countries, or surface feet per minute (SFM) in America. Typical values for cutting speed are 10m/min to 60m/min for some steels, and 100m/min and 600m/min for aluminum. This should not be confused with the feed rate.
- Spindle speed (S): - This is the rotation speed of the tool, and is measured in revolutions per minute (rpm). Typical values are from hundreds of rpm, up to tens of thousands of rpm.
- Diameter of the tool (D):
- Feed per tooth (F_z): - This is the distance the material is fed into the cutter as each tooth rotates. This value is the size of the deepest cut the tooth will make.
- Feed rate (F): - This is the speed at which the material is fed into the cutter. Typical values are from 20mm/min to 5000mm/min.
- Depth of cut: - This is how deep the tool is under the surface of the material being cut (not shown on the diagram). This will be the height of the chip produced. Typically, the depth of cut will be less than or equal to the diameter of the cutting tool.

The machinist needs three values: S, F and Depth when deciding how to cut a new material with a new tool. However, he will probably be given values of V_c and F_z from the tool manufacturer. S and F can be calculated from them:

Spindle Speed	Feed rate
$S = \frac{1000V_C}{\pi D}$	$F = zSF_z$
Looking at the formula for the spindle speed, S, it can be seen that larger tools require lower spindle speeds, while small tools may be able to go at high speeds.	The formula for the feed rate, F shows that increasing S or z gives a higher feed rate. Therefore, machinists may choose a tool with the highest number of teeth that can still cope with the swarf load.

Table 1.2 relation between spindle speed and Feed rate

1.7.6 Selecting a milling cutter

Selecting a milling cutter is not a simple task. There are many variables, opinions and lore to consider, but essentially the machinist is trying to choose a tool which will cut the material to the required specification for the least cost. The cost of the job is a combination of the price of the tool, the time taken by the milling machine, and the time taken by the machinist. Often, for jobs of a large number of parts, and days of machining time, the cost of the tool is lowest of the three costs [11].

Material: - High speed steel (HSS) cutters are the least-expensive and shortest-lived cutters. Cobalt steel is an improvement on HSS and generally can be run 10% faster. Carbide tools are more expensive than steel, but last longer, and can be run much faster, so prove more economical in the long run. HSS tools are perfectly adequate for many applications. The progression from HSS to cobalt steel to carbide could be viewed as very good, even better, and the best.

Diameter: - Larger tools can remove material faster than small ones, therefore the largest possible cutter that will fit in the job is usually chosen. When milling an internal contour,

or concave external contours, the diameter is limited by the size of internal curves. The radius of the cutter must be less than or equal to the radius of the smallest arc.

Flutes: - More flutes allows a higher feed rate, because there is less material removed per flute. But because the core diameter increases, there is less room for swarf, so a balance must be chosen.

Coating: - Coatings, such as Titanium nitride, also increase initial cost but reduce wear and increase tool life.

Helix angle: - High helix angles are typically best for soft metals, and low helix angles for hard or tough metals.

1.8 Design Criteria

An end mill is a cutter of a smaller diameter (usually between 5 mm and 30 mm diameter) clamped in overhang, and its length is several times its diameter. Figure 1.5 shows an end mill with detail geometric properties.

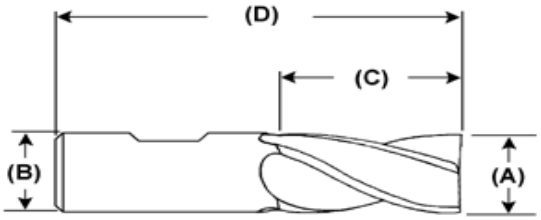

Figure 1.18 Geometric properties of the end mill

A - mill size or cutting diameter B - shank diameter

C - length of cut or flute length D - overall length

- Angular Edge - That cutting edge that is a straight line, forming an angle with the cutter axis. The surface produced by a cutting edge of this type will not be flat as is the case with a helical cutting edge.

- Axial Runout - The difference between the highest and lowest indicator reading taken at the face of a cutter near the outer diameter.
- Chamfer - A short relieved flat installed where the periphery and face of a cutter meet. Used to strengthen the otherwise weak corner.
- Chip Breakers - Special geometry of the rake face that causes the chip to curl tightly and break.
- Chip Splitters - Notches in the circumference of a Corn cob style End mill cutter resulting in narrow chips. Suitable for rough machining.
- Core Diameter - The diameter of a cylinder (or cone shape with tapered End mills) tangent to the flutes at the deepest point.
- Counterbore - A recess in a non-end cutting tool to facilitate grinding.
- Cutter Sweep (Runout) - Material removed by the fluting cutter (or grinding wheel) at the end of the flute.
- Cutting Edge (A) - The leading edge of the cutter tooth. The intersection of two finely finished surfaces, generally of an included angle of less than 90 degrees.
- Cutting Edge Angle - The angle formed by the cutting edge and the tool axis.
- Differential pitch cutters - A specifically designed variation in the radial spacing of the cutter teeth. This provides a variation in tooth spacing and can be beneficial in reducing chatter. This concept is based on reducing the harmonic effect of the tool contacting the part in an exact moment of vibration.
- Entrance Angle - The angle formed by a line through the center of the cutter at 90 to the direction of feed and a radial line through the initial point of contact. As this angle approaches 90 degrees the shock loading is increased.
- Entrance Angle**:** Ramp**-**in - Angle or radius value to enter the cutter into the part surface
- Fillet - The radius at the bottom of the flute, from which core diameter is found.
- Flute - Space between cutting teeth providing chip space and regrinding capabilities. The number of cutting edges. Sometimes referred to as "teeth" or "gullet". The number on an end mill will determine the feed rate.

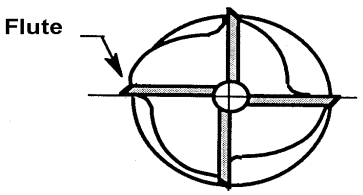

Figure 1.19 Flute

- Flute Length - Length of flutes or grooves. Often used incorrectly to denote cutting length.
- Shank - Projecting portion of cutter which locates and drives the cutter from the machine spindle or adapter
- Straight Shank - Cylindrical shank, with or without driving flats or notches, often seen on carbide end mills
- Weldon Shank - Industry name for a specific type of shank with a drive and location flat. The flat on the cutter provides positive (non slip) driving surface to the End mill.
- Tooth - The cutting edge of the End mill.

Tooth Face - Also known as the Rake Face. The portion of the tooth upon which the tooth meets the part.

1.9 End Mill Technical Features

- Back taper - A slight taper resulting in the shank end of the cutting diameter being smaller than the cutting end. This condition aids not only the plunging or drilling condition but also tends to compensate for deflection.
- Clearance - Space created by the removal of additional tool material from behind the relief angle.

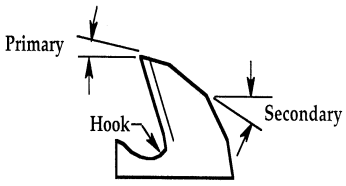

Figure 1.20 Clearance Angle

- Clearance Angle - The angle formed by the cleared surface and line tangent to the cutting edge.
    - Clearance**:** Primary (1st angle, 5°-9°) - Relief adjacent to the cutting edge.
    - Clearance**:** Secondary (2nd angle, 14°-17°) - Relief adjacent to cutting edge
    - Clearance**:** Tertiary (3rd) - Additional relief clearance provided adjacent to the secondary angle.
- Concave - Small hollow required on the end face of an End mill. This feature is produced by a Dish angle produced on the cutter.
- Convex - An outward projection radius feature on the end face of a Ball mill.
- Dish Angle - The angle formed by the end cutting edge and a plane perpendicular to the cutter axis. Dish ensures that a flat surface is produced by the cutter.

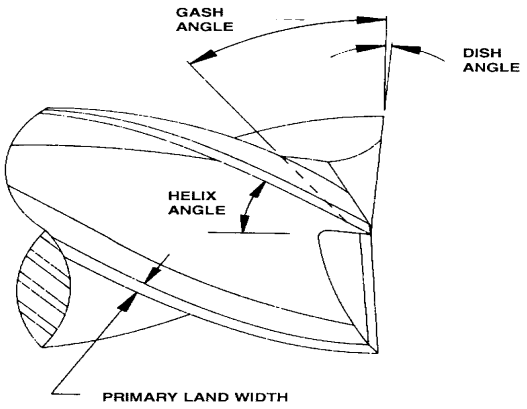

Figure 1.21 Dish Angle, Gash angle, Helix Angle of milling cutter

- Gash (Notch) - The secondary cuts on a tool to provide chip space at corners and ends. The space forming the end cutting edge, which is used when feeding axially.
- Gash angle - The relief angle of the gash feature.
- Gash width - The width of the gash feature. The space between cutting edges, which provides chip space and resharpening capabilities. Sometimes called the flute.
- Heel - The back edge of the relieved land. It is the surface of the tooth trailing the cutting edge.

- Helical - A cutting edge or flute which progresses uniformly around a cylindrical surface in an axial direction. The normal helical direction is a right direction spiral.
- Helix Angle - The angle formed by a line tangent to the helix and a plane through the axis of the cutter or the cutting edge angle which a helical cutting edge makes with a plane containing the axis of a cylindrical cutter.
- Hook - A term used to refer to a concave condition of a tooth face. This term implies a curved surface rather than a straight surface. Hook must be measured at the cutting edge, making measurement difficult.
- Land - The narrow surface of a profile sharpened cutter tooth immediately behind the cutting edge,
    - (A) Cylindrical - a narrow portion of the peripheral land, adjacent to the cutting edge, having no radial relief.
    - (B) Relieved - A portion of the land adjacent to the cutting edge, which provides relief.

Lead - The axial advance of a helical cutting edge in one revolution

Lead = (Cutter diameter x Pi) / Tangent Helix Angle

- Length of Cut (Flute Length) - The effective axial length of the peripheral cutting edge which has been relieved to cut.
- Radial Rake angle - The angle made by the rake face and a radius measured in a plane normal to the axis.

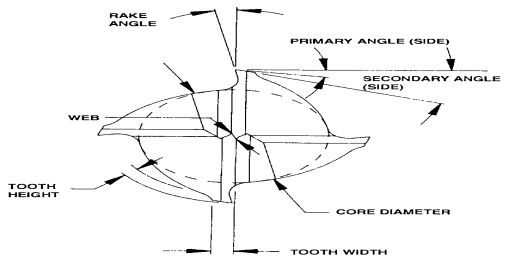

Figure 1.22 Flute in front view

- Rake - The angular relationship between the tooth face or a tangent to the tooth face at a given point and a reference plane or line. An angular feature ground onto the surface of an end mill.
    - Axial rake - The angle formed by a plane passing through the axis and a line coinciding with or tangent to the tooth face.
    - Effective rake - The rake angle influencing chip formation most is that measured normal to the cutting edge. The effective rake angle is greatly affected by the radial and axial rakes only when corner angles are involved.
    - Helical rake - For most purposes the terms helical and axial rake can be used interchangeably. It is the inclination of the tooth face with reference to a plane through the cutter axis.
    - Negative Rake - Exists when the initial contact between tool and workpiece occurs at a point or line on the tooth other than the cutting edge. The rake surface leads the cutting edge.
    - Positive Rake - Exists when the initial contact between the cutter and the workpiece occurs at the cutting edge. The cutting edge leads the rake surface.

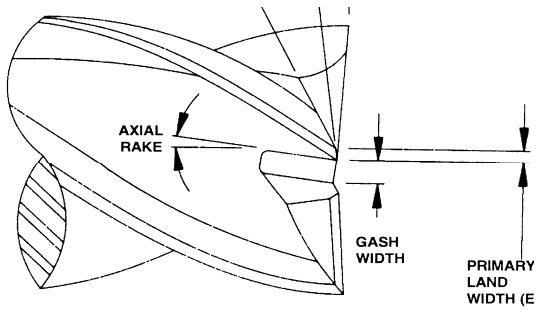

Figure1.23 Rake Angle

- Relief-Space - Provided by removing material immediately behind the cutting edge. Done to eliminate the possibility of heeling or rubbing.
    - Axial angle relief - The angle made by a line tangent to the relieved surface at the end cutting edge and a plane normal to the axis.
    - Axial relief - The relief measured in the axial direction between a plane perpendicular to the axis at the cutting edge and the relieved surface. Helps to prevent rubbing as the corner wears.
    - Concave relief - The relieved surface behind the cutting edge having a concave form. Produced by a grinding wheel set at 90 degrees to the cutter axis.
    - Eccentric relief - The relieved surface behind the cutting edge having a convex form. Produced by a type I wheel presented at an angle to the cutter axis.
    - End relief - Relief on the end of an end mill. Needed only for plunging cutters and to relieve rubbing as the result of corner wear.
    - Flat relief **-** The surface relieved behind the cutting edge having a flat surface produced by the face of a cup wheel**.**

Radial relief - Relief in a radial direction measured in the plane of rotation. It can be measured by the amount of indicator drop at a given radius in a given amount of angular rotation.

Tangential rake angle - The angle made by a line tangent to a hooked tooth at the cutting edge and a radius passing through the same point in plane normal to the axis.

Due to its wide use in industry, milling system is considered. The main concern of this master thesis is the accurate knowledge the static and dynamic properties of machining system components. Generalized equations will present which can be used for predicting the static and dynamic properties. Substructuring methods are used in predicting the total system dynamics based on component analysis.

Static and dynamic properties of machine tool play an important role in a machining process. The knowledge of static and dynamic deflections of the end mill are required to predict the form errors and chatter stability limits in milling without experimental measurements.

Most of these thesis researches have focused on topics such as multimode chattering, variations of machine tools and cutting tools, numerical modeling. However, a thorough discussion of chatter theory and equations, along with improvement to techniques for creating the stability lobe diagram, are equally important.

Excessive forces, deformations and vibrations are experienced during the machining and these problems cause many quality and productivity problems. Process models together with structural models of machining system components need to be integrated into CAD/CAM environment in order to predict and compensate surface errors and determine chatter free machining condition. In a virtual machining system, most of the effects that are observed in real machining could be simulated in advance. This is very important in CAD/CAM systems where part accuracy and the optimal stable cutting conditions can be determined before the machining process.

Therefore, force, form error and stability models can be used to improve productivity, dimensional integrity and surface finish quality in milling operations

CHAPTER TWO
LITERATURE SURVEY

Process modeling is needed for modeling structural properties of milling system components. Modeling of milling process has been the subject of many studies some of which are summarized by Smith and Tlusty (1991). The focus of these studies has mostly been on the modeling of cutting geometry and force, stability and prediction of part quality. Milling forces have been investigated using different approaches. Koenigsberger and Sabberwal (1961) developed equations for milling forces using mechanistic modeling where the cutting force coefficients which relate the chip area to tangential, radial and axial forces are calibrated through force measurements. The mechanistic approach has been widely used for the force predictions and also have been extended to predict associated machine component deflections or surface geometrical errors [Kline et al., 1982**;** Budak and Altintas, 1995]. Another alternative is to use mechanics of cutting approach in determining milling force coefficients as used by Armarego et al. (1985). In this approach, an oblique cutting force model together with an orthogonal cutting database are used to predict milling force coefficients eliminating the need for milling tests as different tool and cutting geometries can be handled by the oblique model [Budak et al. 1996]. Once the cutting force coefficients are known, the milling forces can be determined by integrating the forces along the cutting edges. Altintas et al. (1996, 2001) also demonstrated the application of this approach to complex milling cutter geometries. Milling forces can be used to predict tool and part deflection and form errors. (Figure 2.1)

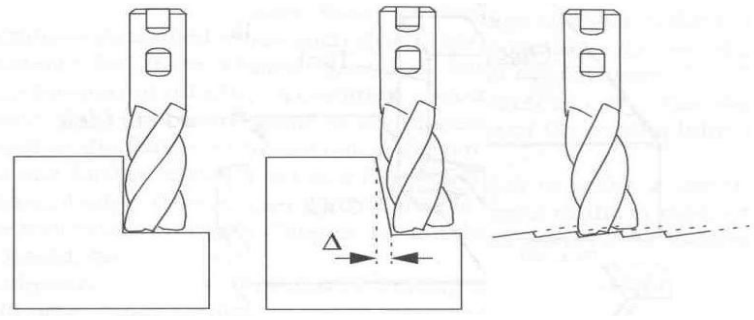

a) Ideal geometry b) Form error c) Surface roughness

Figure 2.1: Effect of tool deflection on form error and surface roughness

Another major limitation on productivity and surface quality in milling is the chatter vibrations which develop due to dynamic interactions between the cutting tool and workpiece, and result in poor surface finish and reduced tool life. Tlusty et al. (1963) and Tobias (1965) identified the most powerful source of self-excitation which is associated with the structural dynamics of the machine tool and the feedback between the subsequent cuts on the same cutting surface resulting in regeneration of waviness on the cutting surfaces, and thus modulation in the chip thickness [Koenigsberger and Tlusty, 1967]. Under certain conditions the amplitude of vibrations grows and the cutting system becomes unstable. Additional operations, mostly manual, are required to clean the chatter marks left on the surface (Figure 2.2). Thus, chatter vibrations result in reduced productivity, increased cost and inconsistent product quality.

Productivity and surface quality in milling processes have direct effects on cost, production lead-time and quality of machined parts. Chatter is one of the most common limitations for productivity and part quality in milling operations. Poor surface finish with reduced productivity and decreased tool life are the usual results of chatter. Additional operations, mostly manual, are required to clean the chatter marks left on the surface. Thus, chatter vibrations result in reduced productivity, increased cost and inconsistent product quality. The importance of modeling and predicting stability in milling has further increased within last couple of decades due to the advances in high speed milling technology. At high speeds, the stabilizing effect of process damping diminishes making process more prone to chatter. On the other hand, high stability limits, usually referred to as stability lobes, exist at certain high spindle speeds which can be used to increase chatter-free material removal rate substantially provided that they are predicted accurately.

Chatter vibrations develop due to dynamic interactions between the cutting tool and workpiece. Under certain conditions the amplitude of vibrations grows and the cutting system becomes unstable. Although chatter is always associated with vibrations, in fact it is fundamentally due to instability in the cutting system. The first accurate modeling of

self-excited vibrations in orthogonal cutting was performed by Tlusty [1] and Tobias [2]. They identified the most powerful source of self-excitation, regeneration, which is associated with the dynamics of the machine tool and the feedback between the subsequent cuts on the same cutting surface. The stability analysis of milling is complicated due to the rotating tool, multiple cutting teeth, periodical cutting forces and chip-load directions, and multi-degree-of-freedom structural dynamics. In the early milling stability analysis, Koenigsberger and Tlusty [3] used the orthogonal chatter model [1] considering an average direction and average number of teeth in cut. An improved approximation was performed by Opitz et al [4]. Sridhar et al. [5, 6] performed a comprehensive analysis of milling stability which involved numerical evaluation of the dynamic milling system's state transition matrix. On a two-degree-of-freedom cutter model with point contact, Minis et al. [7] used Floquet's theorem and the Fourier series for the formulation of the milling stability, and numerically solved it using the Nyquist criterion. Budak [8] developed a stability method which leads to analytical determination of stability limits in milling. The method was verified by experimental and numerical results [9, 10], applied to the stability of ball-end milling [11], and was also extended to 3D milling [12]. The special case of low immersion milling has been investigated

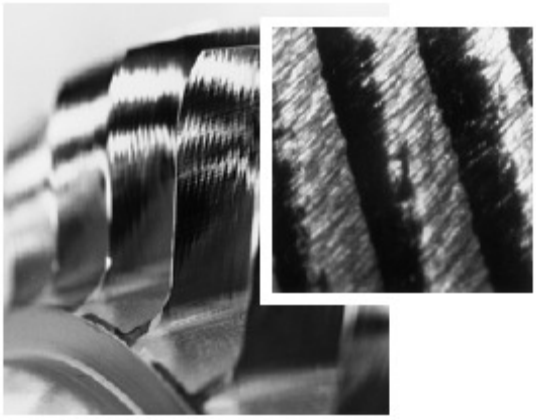

Figure 2.2 Chatter marks on the surface

CAD/CAM is the most common example of computer integration to manufacturing environment promising improved productivity, quality and flexibility. They are the most important elements for development of virtual machining systems. One significant shortcoming of CAD/CAM systems is the fact that they mostly neglect the mechanics of the process when simulating the machining cycles. Many quality and productivity problems such as excessive forces, deformations and vibrations resulting in reduced material removal rates, on the other hand, are experienced during the machining. Process models together with structural models of machining system components need to be integrated into CAD/CAM environment in order to achieve a virtual machining system where most of the effects that are observed in real machining could be simulated in advance.

Demonstrations of cutting model implementation in CAD/CAM systems have been done in several studies [Altintas and Spence, 1991, Yazar et al., 1994]. Altintas and Spence (1991), and Yazar et al. (1994) demonstrated that force models could be used to predict form errors and optimize feedrates based on simulation at the CAD/CAM stage. Weck et al. (1994) demonstrated determination of chatter free milling conditions in a commercial CAD/CAM software. Cutting force coefficients and tool dynamics were needed for these simulations, which were determined experimentally. Generation of an orthogonal cutting database for a work material as Budak et al. (1996) did reduces the amount of experiments, and thus makes implementation of force models in CAD/CAM more practical. There is a need for more practical determination of structural properties of the cutting tool for a virtual machining system. Kops et al. (1990) determined an equivalent diameter for end mill based on FEA in order to be able to use beam equations for deflection calculations, which eliminate stiffness measurements for each tool.

Static and dynamic deformations of machine tool, tool holder and cutting tool play an important role in tolerance integrity and stability in a machining process affecting part quality and productivity. Excessive static deflections may cause tolerance violations whereas chatter vibrations result in poor surface finish. Cutting force, surface finish and cutting stability models can be used to predict and overcome these problems. This would

require static and dynamic data for the structures involved in a machining system [Altintas, 2000]. Considering great variety of machine tool configurations, tool holder and cutting tool geometries, analysis of every case can be quite time consuming and unpractical. These data are usually obtained by testing using stiffness measurements and modal analysis [Altintas, 2000, Budak and Altintas, 1994 and Koenigsberger and Tlusty, 1967].

Recent improvements in machine and spindle designs have led to the increased use of high-speed machining (HSM) in the manufacture of discrete parts [Smith et al., 1998]. It is recognized that a major practical limitation on the productivity of HSM systems is regenerative chatter. Therefore, many studies have explored methods to maximize material removal rate (MRR) during HSM, while avoiding chatter. HSM simulation, which is crucial for pre-process chatter prediction and avoidance, requires knowledge of the system dynamics reflected at the tool point. In general, a separate set of tool point frequency response function (FRF) measurements must be performed for each tool/holder/spindle combination on a particular machining center. These measurements can prove time consuming and lead to costly machine downtime. In order to reduce measurement time and increase process efficiency receptance coupling substructure analysis (RCSA) is used to predict the tool point dynamic response. Building on early work of Duncan (1947), Bishop and Johnson (1960) and more recent work of Ewins (1986) and Ferreira and Ewins (1995). Schmitz and Donaldson (2000) and Schmitz et al. (2001) develop an analytic expression for the frequency response at the free end of the milling cutter from: 1) an analytic model of the tool; 2) an experimental measurement of the holder/spindle sub-assembly; and 3) a set of empirical connection parameters. These parameters are extracted from a single measurement of the tool/holder/spindle assembly at a known tool overhang length using nonlinear least squares estimation [Schmitz and Burn, 2003].

Machining by metal cutting is one of the most popular manufacturing techniques. Over $100 billion is spent annually on machining operations in the United States [13]. High material removal rate (MRR) and surface quality are always the primary objectives of machining operations. Since the 19th century Industrial Revolution, continuous improvements have been made in machine tools and cutting tools. New materials and

designs have significantly increased the hardness and life of cutting tools. High-speed machining centers can now operate at spindle speeds as high as half a million revolutions per minute (RPM). In order to utilize the power and capacity of these new machine tools and cutting tools, and to achieve potential high MRR and desired surface quality, optimum machining parameters are necessary.

Much research has been done on improving the material removal rate and surface quality by setting optimal machining parameters and controlling machine tool chatter. Machine chatter theory was first developed by Tobias & Fishwick [14] in the late 1950s. For half a century, many researchers have contributed to the development of the regenerative chatter theory, including Merritt [15], Tlusty [16, 17], Smith [18], and Altintas & Budak [19]. Regenerative chatter theory creates a relationship between spindle speed and the critical chip width or depth of cut. The theory produces a stability lobe diagram and makes it possible to achieve the highest applicable MRR for a machining process. In the past decade, there have been more than a dozen doctoral dissertations [19-24] and a number of research articles published [25-75].

CHAPTER THREE
PROCESS MODELING IN MILLING

High cutting forces, tool breakage, part and tool deflections and chatter vibrations are the common reasons for reduced productivity and quality in many milling operations. Milling process can be modeled in order to overcome or reduce the effects of these limitations. In this chapter, modeling methods of force, deflection, surface error and stability are presented.

For a stable milling process, milling forces, part and tool deflections can be determined using static analysis. The force predictions can be used to determine structural deformations and form errors left on the finished surface. In the first and second section, force and structural models are described.

Another very important limitation in milling is the self-exited chatter vibrations, which cause poor surface finish and tool life resulting in reduced productivity. In the third section, mathematical models for chatter are presented.

3.1. Milling Force Modeling

Milling forces can be modeled for given cutter geometry, cutting conditions, and work material. The geometry of chip formation and milling force components is shown in Figure 2.1. [Budak, 2002]**.**

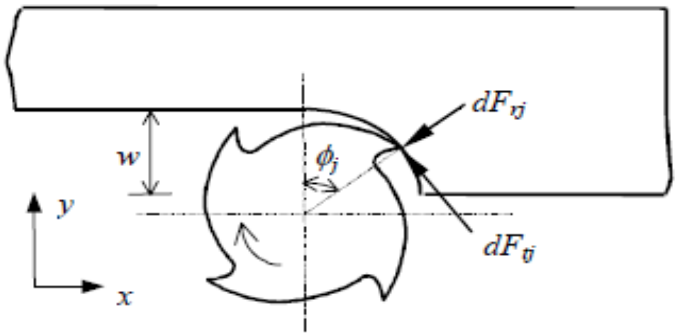

Figure 3.1: Cross sectional view of an end mill showing differential forces

Tangential (dF_t) and radial (dF_r) forces act on a differential flute element with height dz. For a point on the (j^{th}) cutting tooth, differential milling forces in the tangential (dF_t) and radial direction (dF_r) can be given as

$$dF_{t_j}(\phi, z) = K_t h_j(\phi, z)\, dz$$
$$dF_{r_j}(\phi, z) = K_r dF_{t_j}(\phi, z) \qquad 3.1$$

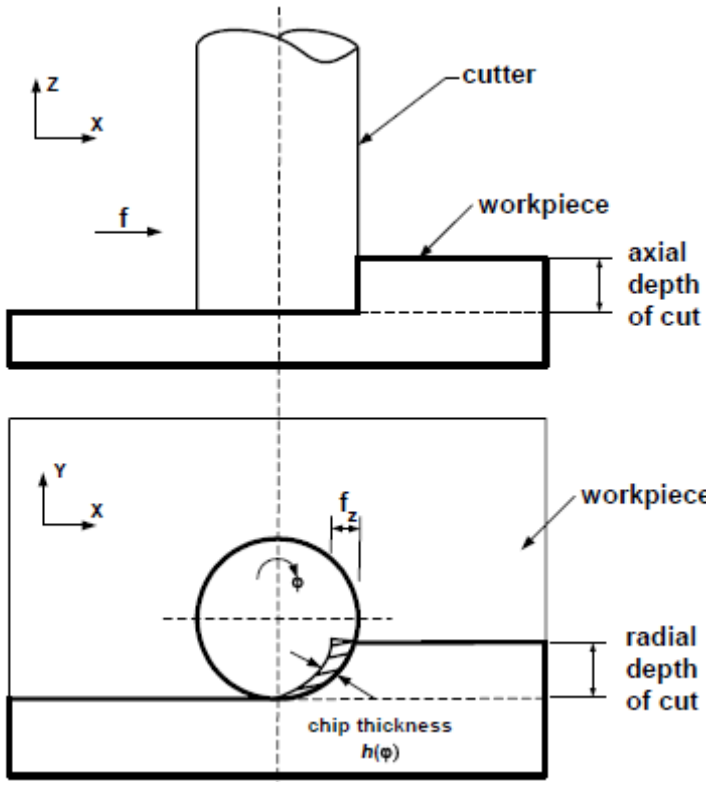

Figure3.2 End Milling Cutting Geometry

where ϕ is the immersion angle measured from the positive *y* axis as shown in Figure 3.1. The radial (*w*) and axial depth of cut (*a*), number of teeth (*N*), cutter radius (*R*) and helix angle (β) determine what portion of a tooth is in contact with the workpiece for a given

angular orientation of the cutter (ϕ). In milling the instantaneous chip thickness variation can be approximated as

$$h_j(\phi, z) = f_t \sin \phi_j(z) \qquad 3.2$$

Where f_t is the feed per tooth (mm/rev-tooth) and $\phi_j(z)$ is the immersion angle for the flute (j) at axial position z.

In equation 3.1 K_t and K_r are the milling force coefficients. All milling force coefficients depend on the workpiece material and cutting tool geometry. In exponential force model, milling force coefficients K_t and K_r can be expressed as exponential functions of the average chip thickness. [Altintas, 2000] In linear force model, both cutting and edge force coefficients are assumed to be independent of the chip thickness.

$$K_t = K_T h_a^{-p};\ K_r = K_R h_a^{-q} \qquad (3.3)$$

where p and q are cutting force constants determined from cutting experiments at different feed rates. Average chip thickness (h_a)

$$h_a = \frac{\int_{\phi_{start}}^{\phi_{exit}} f_t \sin \phi d\phi}{\phi_{exit} - \phi_{start}} \qquad (3.4)$$

In equation (3.1) the edge forces are also included in the cutting force coefficient, which is usually referred to as the exponential force model. They are separated from the cutting force coefficients in edge force or linear force model [Budak, 1994; Budak et al., 1996]:

$$dF_{t_j}(\phi,z)=\left[K_{te}+K_{tc}h_j(\phi,z)\right]dz$$
$$dF_{r_j}(\phi,z)=\left[K_{re}+K_{rc}h_j(\phi,z)\right]\,dz \tag{3.5}$$

where K_{tc} and K_{rc} are the cutting force coefficients contributed by the shearing action in tangential and radial directions, respectively and K_{te} and K_{re} are the edge constants.

Due to the helical flute, the immersion angle changes along the axial direction as

$$\phi_j(z)=\phi+(j-1)\phi_p-\frac{\tan\beta}{R}z \tag{3.6}$$

where the cutter pitch angle (or tooth spacing angle) is defined as $\phi_p = 2\pi/N$. At an axial depth of cut z the lag angle is $\psi = k_\beta z$, where $k_\beta = \tan\beta/R$.

The tangential and radial forces can be resolved in the feed, x, and normal, y, directions using the transformation as follows

$$dF_{x_j}=-dF_{t_j}\cos\phi_j-dF_{r_j}\sin\phi_j$$
$$dF_{y_j}=dF_{t_j}\sin\phi_j-dF_r\cos\phi_j \tag{3.7}$$

The differential cutting forces are integrated analytically along the in-cut portion of the flute j in order to obtain the total cutting force produced by the flute:

$$F_{x,y}\left(\phi_j(Z)\right)=\int_{z_{jl}}^{z_{ju}}dF_{x,y}(\phi_j(z))dz \tag{3.8}$$

where $z_{jl}(\phi_j(z))$ and $z_{ju}(\phi_j(z))$ are the lower and upper axial engagement limits of the contact or the tooth (*j*). The integrations are carried out by noting $\phi_j(z) = \phi + (j-1)\phi_p - k_\beta z$, $d\phi_j(z) = -k_\beta dz$ [Budak and Altintas, 1995]. Thus

$$F_{x_j} = \int_{z_{jl}}^{z_{ju}} (-dF_{t_j}\cos\phi_j - dF_{r_j}\sin\phi_j)dz \tag{3.9}$$

Substituting dF_{t_j} and dF_{r_j} from equation (3.1)

$$F_{x_j} = \int (-K_t f_t \sin\phi_j \cos\phi_j - K_r K_t f_t \sin\phi_j \sin\phi_j)dz \tag{3.10}$$

and substituting

$$\begin{aligned} dz &= -\frac{d\phi_j(z)}{k_\beta} \\ k_\beta &= \frac{\tan\beta}{R} \\ \sin^2\phi_j &= \frac{1+\cos\phi_j}{2} \\ \sin 2\phi_j &= \sin_j \cos\phi_j \end{aligned} \tag{3.11}$$

Then

$$F_{x_j} = \frac{K_t f R_t}{4\tan\beta}[-\cos 2\phi_j + (2\phi_j(z) - \sin 2\phi_j(z))]_{Z_{jl(\phi)}}^{Z_{ju(\phi)}} \tag{3.12}$$

and

$$F_{y_j} = \int (dF_{t_j}\sin\phi_j - dF_{r_j}\cos\phi_j)d_z \tag{3.13}$$

By substituting the above equations

$$F_{y_j} = -\frac{K_t f_t R}{4\tan\beta}[(2\phi_j(z) - \sin 2\phi_j(z)) + K_r \cos 2\phi_j(z)]_{z_{jl}(\phi)}^{z_{ju}(\phi)} \tag{3.14}$$

$$F_{x_j}(\phi) = \frac{K_t f_t R}{4\tan\beta}[-\cos 2\phi_j + k_r(2\phi_j(z) - \sin 2\phi_j(z))]_{z_{jl}(\phi)}^{z_{ju}(\phi)}$$

$$F_{y_j}(\phi) = -\frac{K_t f_t R}{4\tan\beta}[(2\phi_j(z) - \sin 2\phi_j(z)) + K_r \cos 2\phi_j(z)]_{z_{jl}(\phi)}^{z_{ju}(\phi)} \qquad (3.15)$$

The cutting forces contributed by all flutes are calculated and summed to obtain the total instantaneous forces on cutter at immersion ϕ:

$$F_x(\phi) = \sum_{j=1}^{N} F_{x_j}(\phi);$$

$$F_y(\phi) = \sum_{j=1}^{N} F_{y_j}(\phi) \qquad (3.16)$$

3.2. Tool Deflection and Form Error

In end milling, the finished workpiece surface is perpendicular to the direction of feed. If feed and normal directions are aligned with Cartesian x and y axes respectively, any deflection in the y-axis may produce a static form error. End mills can be considered as elastic cylinder beam, cantilevered to the spindle through collet end chuck. Flexible cutters deflect under the periodically varying milling forces, which are modeled in the previous section.

Generating the surface becomes complex when the end mill has helical flutes. The cutting forces are not constant but vary with the rotation of the end mill. Furthermore, the helix angle of the flutes produces additional variation on distribution of cutting forces along the z-axis. As the end mill rotates, the tip of the flute moves to immersion ϕ. Since the normal cutting force will not be zero at this instant, the elastic end mill displacement will produce a form error on the surface. Depending on the number of flutes and width of cut, there may be more than one cutting edge point in contact with the finish surface.

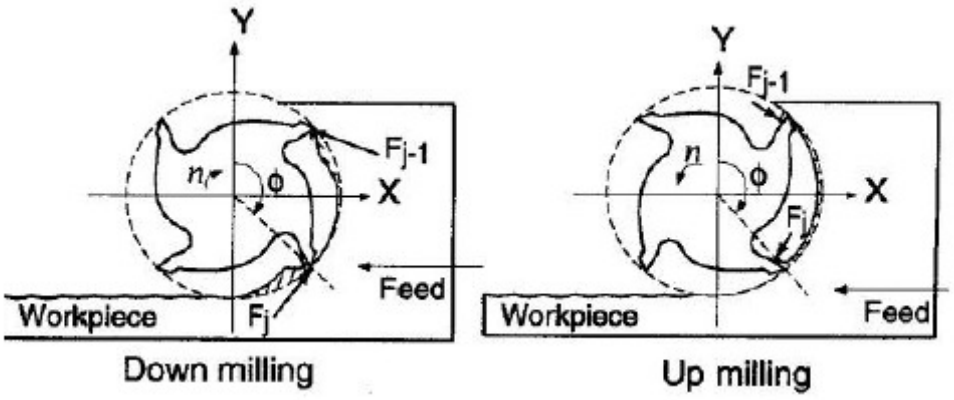

Figure 3.3 The influence of the milling mode on the surface form errors

The contact points can be calculated by equating the instantaneous immersion angle $\phi_j(z)=\phi+(j-1)\phi_p-k_\beta z$, with k_β=tanβ/*R* to zero in up milling and to π in down milling.

$$z=\frac{\phi+(j-1)\phi_p}{k_\beta}\ \text{(Up milling)};\quad z=\frac{\pi-(\phi+(j-1)\phi_p)}{k_\beta}\ \text{(down milling)},j=1,2..N-1 \quad (3.17)$$

where β is the helix angle and $\phi_p=(2\pi)/N$ is the cutter pitch angle. The cutter can be divided into *M* number of small disk elements within the axial depth of cut (*a*) and it can be rotated at increments $\Delta\phi$, (i.e., ϕ=0, $\Delta\phi$, $2\Delta\phi$,..., ϕ_P) (Figure 3.4) [Altintas, 2000].
Figure 3.4:

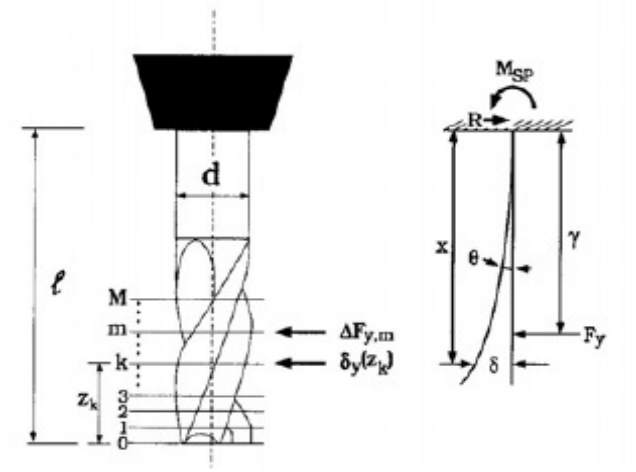

Figure 3.4 Static deformation model of an end mill

Each differential element has an axial depth of cut $(\Delta z = a/M)$, and the influence of the helix angle may be neglected by selecting small elements. The differential cutting force produced by element *m* is given by

$$\Delta F_{y,m}(\phi) = K_t f_t \Delta z \sum_{j=0}^{N-1} \left[\sin\phi_j(z) - K_r \cos\phi_j(z)\right] \sin\phi_j \tag{3.18}$$

where K_t and K_r are cutting constants and f_t is the feed rate per tooth.

The immersion angle for the element *m* is $\phi_j(m) = \phi + (j\text{-}1)\phi_p - k_\beta .m\Delta z$. The deflection in the y direction at the contact point z_k caused by the force applied at the element *m* is given by the cantilever beam formulation. As

$$\delta_y(z_k, m) = \begin{cases} \dfrac{\Delta F_{y,m} v_m^2}{6EI}(3v_m - v_k), & 0 < v_k < v_m \\ \dfrac{\Delta F_{y,m} v_m^2}{6EI}(3v_k - v_m), & v_m < v_k \end{cases} \tag{3.19}$$

where *E* is the young modulus, *I* is the area of inertia of the tool and $v_k = l - z_k$, with *l* being the gage length of the cutter measured form the collet face. The calculation of the area moment inertia of the tool with flute will be explained in chapter 4. The total static deflection at axial contact point z_k is calculated by superposition of the deflections produced by all *M* elemental forces on the end mill:

$$\delta_y(z_k) = \sum_{m=1}^{M} \delta_y(z_k, m) \tag{3.20}$$

At the points where the cutting edges is contact with the finish surface, the deflection $\delta_y(z_k)$ is imprinted as a dimensional error on the workpiece.

3.3. Milling Stability

Chatter in milling has been modeled analytically by considering the regeneration in chip thickness and the machine-process interactions. Milling cutters can be considered to have two orthogonal degrees of freedom as shown in Figure 3.5. [Altintas, 2000]

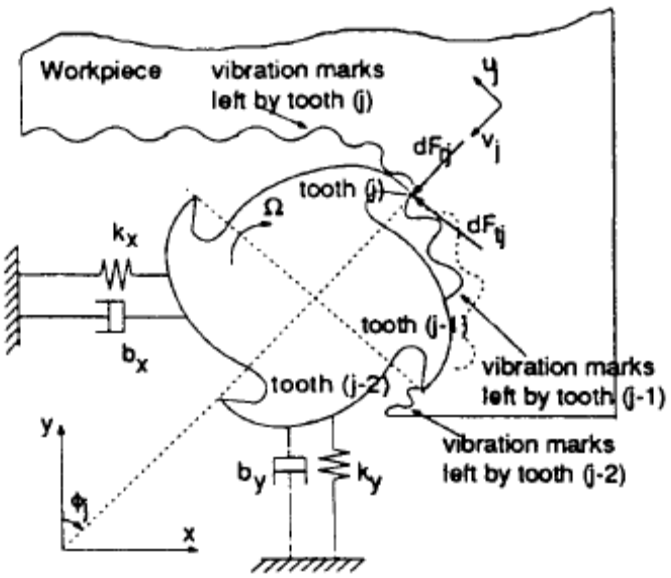

Figure 3.5 Chatter model for milling.

Milling forces excite both cutter and workpiece causing vibrations, which are imprinted on the cutting surface. Each vibrating cutting tooth removes the wavy surface left from the previous tooth resulting in modulated chip thickness, which can be expressed as follows:

$$h_j(\phi) = f_t \sin\phi_j + (\nu^o_{j_c} - \nu^o_{j_w}) - (\nu_{j_c} - \nu_{j_w}) \tag{3.21}$$

where the feed per tooth f_t represents the static part of the chip thickness, and $\phi = \Omega.t$ is the angular position of the cutter measured with respect to the first tooth and corresponding to the rotational speed Ω (rad/sec). In the equation 3.21, *c* and *w* indicate cutter and workpiece, respectively. ν_j and ν^o_j are the dynamic displacements due to tool and workpiece vibrations for the current and previous tooth passes, and include tool and workpiece vibrations. The static part in equation is neglected in the stability analysis. Then the dynamic chip thickness can be put in the following form

$$h_j(\phi) = \left[\Delta x \sin\phi_j + \Delta y \cos\phi_j\right] \tag{3.22}$$

Where

$$\Delta x = (x_c - x_c^o) - (x_w - x_w^o)$$
$$\Delta y = (y_c - y_c^o) - (y_w - y_w^o)$$

where (x_c, y_c) and (x_w, y_w) are the dynamic displacements of the cutter and workpiece in *x* and *y* directions, respectively. Similar to the static force analysis, dynamic cutting forces can be obtained using the dynamic chip thickness as

$$\begin{Bmatrix} F_x \\ F_y \end{Bmatrix} = \frac{1}{2} a K_t \begin{bmatrix} a_{xx} & a_{xy} \\ a_{yx} & a_{yy} \end{bmatrix} \begin{Bmatrix} \Delta x \\ \Delta y \end{Bmatrix} \tag{3.23}$$

where the directional coefficients are given as:

$$\begin{aligned} a_{xx} &= -\sum_{j=1}^{N} \sin 2\phi_j + K_r (1 - \cos 2\phi_j) \\ a_{xy} &= -\sum_{j=1}^{N} (1 + \cos 2\phi_j) + K_r \sin 2\phi_j \\ a_{yx} &= -\sum_{j=1}^{N} -(1 - \cos 2\phi_j) + K_r \sin 2\phi_j \\ a_{yy} &= -\sum_{j=1}^{N} -\sin 2\phi_j + K_r (1 + \cos 2\phi_j) \end{aligned} \tag{3.24}$$

The directional coefficients, *a*, depend on the angular position of the cutter which makes equation (3.23) time-varying:

$$\{F(t)\} = \frac{1}{2} a K_t [A(t)]\{\Delta(t)\} \tag{3.25}$$

$[A(t)]$ is periodic at the tooth passing frequency $\omega = N\Omega$ and with corresponding period of $T = 2\pi/\omega$. In general, Fourier series expansion of the periodic term is used for the solution of the periodic systems. The higher harmonics do not affect the accuracy of the predictions, and it is sufficient to include only the average term in the Fourier series expansion of the periodic terms [Budak et al., 1994; 1998]. As the directional coefficients are valid within the cutting zone between start and exit immersion angles (ϕ_{st}, ϕ_{ex}):

$$[A_0] = \frac{1}{\phi_P} \int_{\phi_{st}}^{\phi_{ex}} [A(\phi)] d\phi = \frac{N}{2\pi} \begin{bmatrix} \alpha_{xx} & \alpha_{xy} \\ \alpha_{yx} & \alpha_{yy} \end{bmatrix} \tag{3.26}$$

where

$$\begin{aligned}
\alpha_{xx} &= \frac{1}{2}\left[\cos 2\phi - 2K_r\phi + K_r \sin 2\phi\right]_{\phi_{st}}^{\phi_{ex}} \\
\alpha_{xy} &= \frac{1}{2}\left[-\sin 2\phi - 2\phi + K_r \cos 2\phi\right]_{\phi_{st}}^{\phi_{ex}} \\
\alpha_{yx} &= \frac{1}{2}\left[-\sin 2\phi + 2\phi + K_r \cos 2\phi\right]_{\phi_{st}}^{\phi_{ex}} \\
\alpha_{yy} &= \frac{1}{2}\left[-\cos 2\phi - 2K_r\phi - K_r \sin 2\phi\right]_{\phi_{st}}^{\phi_{ex}}
\end{aligned} \tag{3.27}$$

Substituting equation (3.26-27) into equation 3.25 and assuming harmonic functions for dynamic forces and vibrations, the characteristics equation is obtained as

$$\det[[I] + \Lambda[G_O(i\omega_c)]] = 0 \tag{3.28}$$

where *[I]* is the unit matrix, and the oriented transfer function matrix is defined as:

$$\begin{aligned}
[G_O] &= [A_O]\,[G] \\
[G(i\omega_c)] &= [G_C(i\omega_c)] + [G_w(i\omega_c)] \\
[G_p] &= \begin{bmatrix} G_{p_{xx}} & G_{p_{xy}} \\ G_{p_{yx}} & G_{P_{YY}} \end{bmatrix} \qquad (p = c, w)
\end{aligned} \tag{3.29}$$

and the eigenvalue (Λ) in equation (3.28) is given as

$$\Lambda = -\frac{N}{4\pi} K_t a (1 - e^{-i\omega_c T}) \tag{3.30}$$

If the eigenvalue Λ is known, the stability limit can be determined from equation (3.30). Λ Can easily be computed from equation (3.28) numerically. However, an analytical solution is possible if the cross transfer functions, G_{xy} and G_{xy}, are neglected in equation (3.28):

$$\Lambda = \frac{1}{2a_0}(a_1 \pm \sqrt{a_1^2 - 4a_0}) \tag{3.31}$$

where

$$\begin{aligned} a_0 &= G_{xx}(i\omega_c)G_{yy}(i\omega_c)(\alpha_{xx}\alpha_{yy} - \alpha_{xy}\alpha_{yx}) \\ a_1 &= \alpha_{xx}G_{xx}(i\omega_c) + \alpha_{yy}G_{yy}(i\omega_c) \end{aligned} \tag{3.32}$$

Since the transfer functions are complex, Λ will have complex and real parts. The axial depth of cut (a) is a real number. When $\Lambda = \Lambda_R + i\Lambda_I$ and $e^{-iw_cT} = \cos w_cT - i\sin w_cT$ are substituted in equation 3.24, the complex part of the equation has to vanish yielding

$$k = \frac{\Lambda_I}{\Lambda_R} = \frac{\sin w_cT}{1 - \cos w_cT} \tag{3.33}$$

The above can be solved to obtain a relation between the chatter frequency and the spindle speed [Budak et al., 1995; 1998]:

$$\begin{aligned} &\omega_cT = \varepsilon + 2k\pi \\ &\varepsilon = \pi - 2\psi; \quad \psi = \tan^{-1} k \\ &n = \frac{60}{NT} \end{aligned} \tag{3.34}$$

where ε is the phase difference between the inner and outer modulations, k is an integer corresponding to the number of vibration waves within a tooth period, and n is the spindle speed (rpm). After the imaginary part in equation (3.30) is vanished, the following is obtained for the stability limit [Budak and Altintas, 1995; 1998]:

$$a_{\lim} = -\frac{2\pi\Lambda_R}{NK_t}(1 - k^2) \tag{3.35}$$

Equations (3.34-35) can be used to determine the stability limit and corresponding spindle speed. When this procedure is repeated for a range of chatter frequencies and number of vibration waves, k, and the stability lobe diagram for a milling system is obtained.

3.4. Importance of the Static and Dynamic Properties of Cutting Tools

Static and dynamic properties of machine tool play an important role in a machining process. The knowledge of static and dynamic deflections of the end mill are required to predict the form errors and chatter stability limits in milling without experimental measurements. Excessive forces, deformations and vibrations are experienced during the machining and these problems cause many quality and productivity problems. Process models together with structural models of machining system components need to be integrated into CAD/CAM environment in order to predict and compensate surface errors and determine chatter free machining condition. In a virtual machining system, most of the effects that are observed in real machining could be simulated in advance. This is very important in CAD/CAM systems where part accuracy and the optimal stable cutting conditions can be determined before the machining process.

Therefore, force, form error and stability models can be used to improve productivity, dimensional integrity and surface finish quality in milling operations

3.5. Summary

In this chapter, milling process models are reviewed. These models can be used in optimization of milling operations. Deflection and surface generation model is used to predict form error. Stability lobes are obtained by using chatter model in order to determine suitable spindle speed. Importance of the static and dynamic properties of tool is emphasized.

CHAPTER FOUR

MODELING OF END MILL STATICS

Static deflection of end mills may cause tolerance violation on milled parts. These deflection need to be modeled in order to check the tolerance integrity for potential compensation of the errors. This chapter covers the static analysis of typical 2-Flute, 3-Flute and 4-Flute end mills. A cantilever beam model is used to perform the static analysis of the cutters under load. Therefore, the primary objective of the static analysis is to determine the maximum deflection at the tool tip.

In the end milling process the deflection of the cutter is an important factor affecting the accuracy of machining, with implications on the selection of cutting parameters and economics of the operation. Although the deflection affects adversely the accuracy, the flexibility of the cutter is beneficial in attenuating the overload in a sudden transient situation, as well as attenuating chatter. The end mill deflection is important to evaluate surface error.

First section of the chapter gives a brief explanation of geometric properties and analytical deflection formulas for cutters; Finite Element Analysis (FEA) results of the tool and tool holder are explained in the second section, which is followed by simplified equations for tool deflection.

4.1. Geometric Parameters and Analytical Statistical Analysis

In order to perform static analysis, models of the 2-Flute, 3-Flute and 4-Flute cutters are needed to determine the necessary geometric and loading parameters, moment of inertia and bending moments. Three models have been developed to determine the maximum deflection using cantilever method of 2-Flute, 3-Flute and 4-Flute cutters since their geometry are different. Their bending moment distributions are the same since they share same loading and boundary conditions. The loading and boundary conditions of the cantilever beam are depicted in Figure 3.1, where *D1* is the mill diameter, *D2* is the shank

diameter, *L1* is the flute length, *L2* is the overall length, *F* is the point load, *I1* is the moment of inertia of the part with flute and *I2* is the moment of inertia of the part without flute. The cutting force is represented by a point force, which is an approximation. However, it should be noted that this model is used only for stiffness calculation, not for final tool deflection. Accurate surface generation models can be used [Budak and Altintas, 1994] for form errors, once the stiffness is determined.

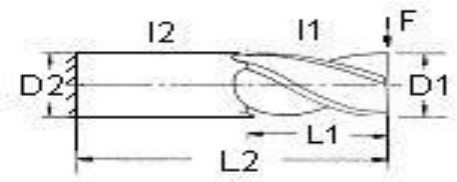

Figure 4.1: Loading and boundary conditions of the end mill

4.1.1. Moment of Inertia

In order to perform the analytic static analysis, models of the 4-Flute, 3- Flute and 2-Flute end mills are needed to determine the moment of inertias. Due to the complexity of the cutter cross-sections its axis, the calculation of the inertia is the most difficult aspect of the static analysis. The cross sections of the 3-Flute, 4- Flute and 2-Flute end mills are as shown in Figure 3.2, where f_d is the flute depth. In the case of the 3-Flute cutters, the shapes of the regions labeled '1' is bounded by the lines x=0, y=-0.5774x and arcs. The region labeled '2' is bounded by the lines x=0, y=0.5774x and an arc. Lastly, the region labeled '3' is bounded by the lines y=0.5774x, y=-0.5774x and an arc. Regions labeled '1', '2', '3' and '4' in the case of the 4-Flute cutters, are bounded by arcs and the lines x=0 and y=0. Regions labeled '1' or '2' in the cross section of the 2-Flute cutter, are bounded by the line y=0. Based on the equations bounding each region, the inertia can be derived. The derivations of the moment of inertia of the 3-Flute, 4- Flute and 2-Flute cutters are provided in Sections 4.1.1.1, 4.1.1.2 and 4.1.1.3. The flute depth, f_d, is in general different for different end mill generation.

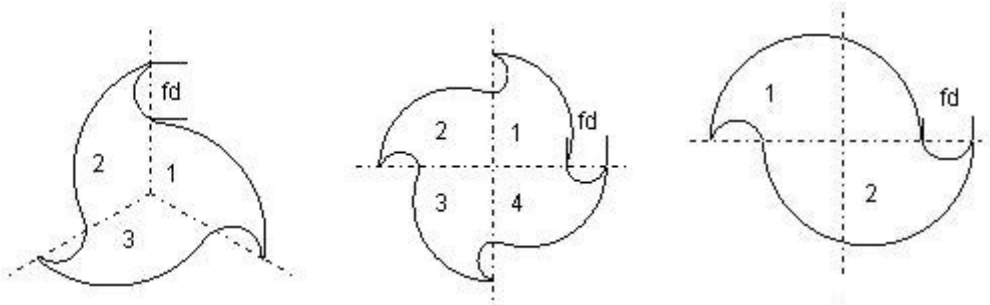

Figure 4.2 Cross-sections of the 3-Flute, 4-Flute and 2-Flute end mills

4.1.1.1. 3-Flute Cutters

In order to obtain the inertia of the cross section, inertia of region 1 is first derived and the inertia of regions 2 and 3 are obtained by transforming the inertia matrix of region 1. The total inertia of cross section is then obtained by summing the inertia of regions 1, 2 and 3.

Using tensor analysis, the inertia of region 2 of a 3-Flute cutter can be obtained by transforming the inertia matrix of region 1, I_1, by 120 degrees as:

$$I_2 = T\, I_1\, T^T \tag{4.1}$$

where the inertia matrices I_1, I_2 and the transformation matrix T are defined as

$$I_1 = \begin{pmatrix} I_{xx,1} & -I_{xy,1} \\ -I_{xy,1} & I_{yy,1} \end{pmatrix}$$
$$I_2 = \begin{pmatrix} I_{xx,2} & I_{xy,2} \\ I_{xy,2} & I_{yy,2} \end{pmatrix} \tag{4.2}$$
$$T = \begin{pmatrix} \cos(\frac{2\pi}{3}) & -\sin(\frac{2\pi}{3}) \\ \sin(\frac{2\pi}{3}) & \cos(\frac{2\pi}{3}) \end{pmatrix}$$

Similarly, the inertia of region 3 can be found by transforming the inertia of region 1 by 240 degrees. That is

$$I_3 = T\, I_1\, T^T \tag{4.3}$$

where the transformation matrix T in this case is defined as

$$T = \begin{pmatrix} \cos(\frac{4\pi}{3}) & -\sin(\frac{4\pi}{3}) \\ \sin(\frac{4\pi}{3}) & \cos(\frac{4\pi}{3}) \end{pmatrix} \tag{4.4}$$

Then, the total inertia of the 3-Flute cutter can be calculated as

$$I_{xx3-flute,TOTAL} = I_{yy3-flute,TOTAL} = 1.5I_{xx,1} + 1.5I_{yy,1} \tag{4.5}$$

The cross section of the region 1 of the 3-Flute cutter is drawn as shown in Figure 3.3

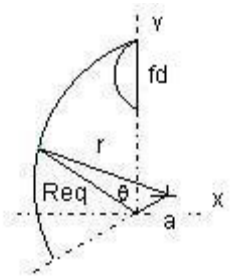

Figure 4.3: Region 1 of 3-Flute end mill

The inertia of region 1 is derived by, first computing the equivalent radius R_{eq} of the arc respect to x- and y-axes by using the cosine law, in terms of the radius r of the arc, position of the center of the arc (a) and θ. (Nermes et al., 2001)

$$R_{eq3-flute}(\theta) = a.\cos(\theta + \frac{\pi}{3}) + \sqrt{(r^2 - a^2) + a^2.\cos^2(\theta + \frac{\pi}{3})} \qquad 0 < \theta < \frac{2\pi}{3} \tag{4.6}$$

The moment of inertia about x-axis and y-axis are given as

$$I_{xx,1} = \int_0^{2\pi/3} \int_0^{R_{eq}(\theta)} \rho^3 \sin^2(\theta) d\rho\, d\theta - \left[\frac{1}{8}\pi(\frac{fd}{2})^4 + \frac{\pi(\frac{fd}{2})^2}{2}(\sqrt{r^2 + a^2} - \frac{fd}{2})^2 \right] \tag{4.7}$$

$$I_{yy,1} = \int_0^{2\pi/3} \int_0^{R_{eq}(\theta)} \rho^3 \cos^2(\theta) d\rho\, d(\theta) - \left[\frac{1}{8}\pi(\frac{fd}{2})^4 \right]$$

Performing the first integral with respect to ρ and rearranging, equation. (4.7) becomes

$$I_{xx,1} = \frac{1}{4}\int_0^{2\pi/3} R_{eq}^4 \sin^2(\theta) d(\theta) - \left[\frac{1}{8}\pi(\frac{fd}{2})^4 + \frac{\pi(\frac{fd}{2})^2}{2}(\sqrt{r^2+a^2} - \frac{fd}{2})^2\right]$$
$$I_{yy,1} = \frac{1}{4}\int_0^{2\pi/3} R_{eq}^4 \cos^2(\theta) d(\theta) - \left[\frac{1}{8}\pi(\frac{fd}{2})^4\right] \quad (4.8)$$

Substituting $R_{eq3-flute}$ (4.6) into integrals and integrating we get the moment of inertia

About x-axis and y-axis for region 1of the 3-Flute end mill. $I_{xx,1}$ and $I_{yy,1}$ are used to evaluate the total moment of the inertia (4.5).

4.1.1.2. 4-Flute Cutters

In the case of the 4-Flute cutters, the cross section of the region 1 is drawn as shown in Figure 4.4. The regions 1, 2, 3 and 4 are symmetrical, therefore the inertia of only one region is necessary to compute and the inertias of the other regions are deduced. For instance, it can be shown that the inertia of region 1 about the x-axis, $I_{XX,1}$, is equal to the inertia of region 2 about the y-axis, $I_{yy,2}$. The total inertia as function of the inertia of the region 1 is found as

$$I_{xx4-flute,TOTAL} = I_{yy4-flute,TOTAL} = 2I_{XX,1} + 2I_{yy,1} \quad (4.9)$$

The inertia of region 1 is derived by, computing the equivalent radius R_{eq} of the arc with respect to x- and y-axes by using the cosine law in terms of r, a and θ

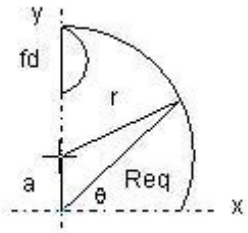

Figure 4.4: Region 1 of 4-Flute end mill

The equivalent radius formula for region 1 of 4-Flute end mill with respect to x- and y-axes is given as follows

$$R_{eq4-flute}(\theta) = a.\sin(\theta) + \sqrt{(r^2 - a^2) + a^2.\sin^2(\theta)} \qquad 0 < \theta \le \frac{\pi}{2} \tag{4.10}$$

The moment of inertia about x-axis and y-axis are found as

$$I_{xx,1} = \frac{1}{4}\int_0^{\pi/2} {R_{eq}}^4 \sin^2(\theta)d\theta - \left[\frac{1}{8}\pi(\frac{fd}{2})^4 + \frac{\pi(\frac{fd}{2})^2}{2}.(r + a - \frac{fd}{2})^2\right]$$
$$I_{yy,1} = \frac{1}{4}\int_0^{\pi/2} {R_{eq}}^4 \cos^2(\theta)d\theta - \left[\frac{1}{8}\pi(\frac{fd}{2})^4\right] \tag{4.11}$$

Substituting $R_{eq4-flute}$ (4.10) into integrals and integrating we obtain $I_{xx,1}$ and $I_{yy,1}$ and they are used to evaluate the total moment of the inertia (4.9).

4.1.1.3. 2-Flute Cutters

In the case of the 2-Flute cutters, the cross section of the region 1 is drawn as shown in Figure 3.5. The cross section of the 2-Flute cutter is not symmetric with respect to x and y-axes, so the total moment of inertia I_{xx} and I_{yy} are different. After transforming and summing, the total moment of inertia of the 2-Flute end mill is found as

$$I_{xx2-flute,TOTAL} = 2I_{xx,1}, I_{yy2-flute,TOTAL} = 2I_{yy,1} \tag{4.12}$$

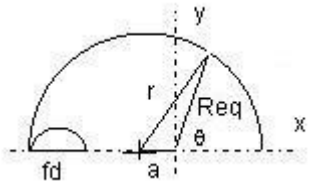

Figure 4.5: Region 1 of 2-Flute end mill

The inertia of region 1 of the 2-Flute cutter is derived by computing the equivalent radius R_{eq} by using the cosine law in terms of r, a and θ.

$$R_{eq2-flute}(\theta) = -a.\cos(\theta) + \sqrt{(r^2 - a^2) + a^2.\cos^2(\theta)} \qquad 0 < \theta < \pi \tag{4.13}$$

The moment of inertia about x- and y-axes are given as

$$I_{xx,1} = \frac{1}{4}\int_0^{\pi} R_{eq}{}^4 \sin^2(\theta) d\theta - \left[\frac{1}{8}\pi(\frac{fd}{2})^4\right]$$
$$I_{yy,1} = \frac{1}{4}\int_0^{\pi/2} R_{eq}{}^4 \cos^2(\theta) d\theta - \left[\frac{1}{8}\pi(\frac{\pi(\frac{fd}{2})^2}{2}) + \frac{\pi(\frac{fd}{2})^2}{2}.(r - \frac{fd}{2})^2\right] \tag{4.14}$$

We obtain $I_{xx,1}$ and $I_{yy,1}$ by substituting $R_{eq2-flute}$ (4.13) into integrals and integrating. They are used to evaluate the total moment of the inertia (4.12).

4.1.2. Maximum Deflection

Knowing the moment of inertia of the 4-Flute, 3- Flute and 2-Flute end mills, the deflection along the length of cutters can be calculated for given material properties (E, elastic modulus) and force (F). Based on the loading conditions, the deflection along the beam is determined by using the moment area theorems. For example, Figure 4.6 shows the variation along two parts of a beam of the quantity M/EI, obtained by dividing the bending moment M by the flexural rigidity EI (Elastic Modulus* Moment of Inertia).

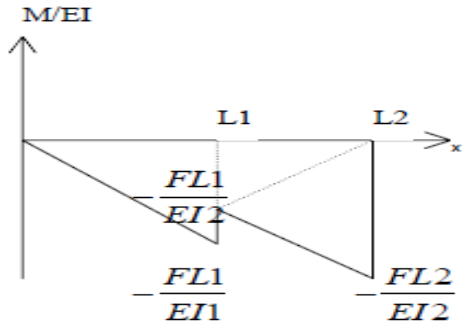

Figure 4.6: Bending moment (ME/I) diagram of the end mill

The product of the area, which refers to the area under the M/EI diagram, and the distance from its centroid to origin gives the maximum deflection at the end point. From Figure 4.6 using moment area method we can define $y_{\max}$ for the end point [Beer and Johnston, 1992].

$$y_{\max} = \frac{FL1^3}{3EI1} + \frac{1}{6}\frac{FL1(L2-L1)(L2+2L1)}{EI2} + \frac{1}{6}\frac{FL2(L2-L1)(2L2+L1)}{EI2} \tag{4.15}$$

4.2. Modeling and FEA Analysis

For parametric, geometric solid modeling and Finite Element Modeling (FEM) several software, such as CATIA, Pro/Engineer, ANSYS and I-DEAS, can be used. For this research, ANSYS is used for geometric modeling and FEM.

4.2.1. Tool

4.2.1.1. Parametric Geometric Modeling

For geometric modeling of 4-Flute, 3-Flute and 2-Flute, helical end mills, ANSYS is a powerful parametric design tool. ANSYS is a Computer Aided Engineering package used to create three-dimensional (3D) solid models of parts. ANSYS is a parametric solid modeling system that makes design changes easy to oerform. Parametric means that the shape of the part is driven by its feature dimensions. Feature dimensions can be redefined at anytime. Many 3D solid models were prepared for end mills with different flute diameter, shank diameter, flute length, overall length and flute number.

4.2.1.2. Finite Element Modeling (FEM) and Analysis (FEA)

Finite element modeling and analysis are performed on ANSYS FE package [Shih, 2000]. End mills are made from high-speed steel (HSS) and carbide that have the following properties necessary to calculate the maximum deflection.

Material	Modulus o Elasticity (GPa)	Poisson's ratio	Density (Kg/m^3)
HSS	200	0.3	8600
Carbide	605	0.3	12500

Table 4.1: Mechanical properties of the tool materials

The 4-Flute, 3-Flute and 2-Flute end mills are meshed with solid linear tetrahedral elements. The end mill is split into two segments: one which represents the shank with one length of elements and another which represents the part including Flute and cutting edges with a second length of elements. This is to reduce the total number of elements suitable for FE analysis.

The end mill is constrained at the end of the shank where it is gripped by the tool holder. The displacement is constrained at that point in all directions. This is actually a simple cantilever beam clamped at one end and free at the other end. The force is applied at the free end. Figure 4.7 illustrates an example of the meshed 3-Flute end mill including boundary conditions. Figure4.7

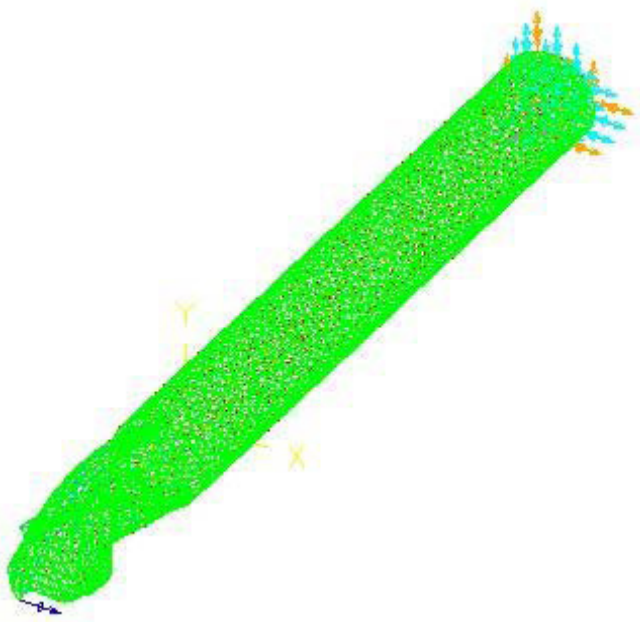

Figure4.7: Meshing and boundary conditions example

Finite Element Analysis (FEA) is applied to great variety of tool geometries and two different tool materials in ANSYS. An example deflection of an end mill is shown in Figure 4.8. Some of the deflection values found by analytic equations (y_{max}, Efunda) and ANSYS are shown in Table 4.2. Approximately sixty tools were tested.

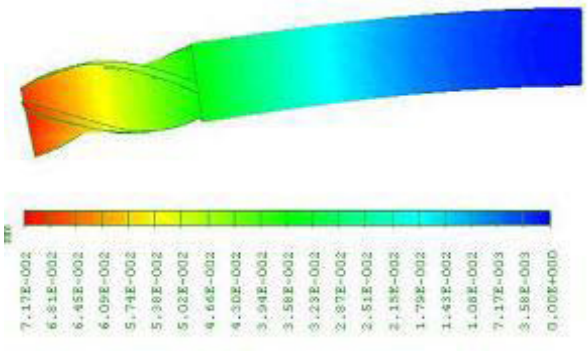

Figure 4.8: Example tool deflection

Flute	Material	D1 (mm)	D2 (mm)	L1 (mm)	L2 (mm)	y-Analy(mm) Force=50N	y-ANSYS Force=50N	Difference (%)
4	HSS	6	6	13	57	0.248844	0.251768	1.16
3	HSS	6	6	13	57	0.245466	0.250252	1.91
2	HSS	6	6	13	57	0.244309	0.249888	1.23
4	HSS	10	10	22	72	0.067320	0.069073	2.54
3	HSS	10	10	22	72	0.065174	0.067203	3.02
2	HSS	10	10	22	72	0.064452	0.066813	3.53
4	HSS	10	13	22	72	0.027316	0.028412	3.86
3	HSS	10	13	22	72	0.024169	0.026517	5.08
2	HSS	10	13	22	72	0.024448	0.026007	5.99
4	HSS	10	10	26	72	0.069894	0.071800	2.65
3	HSS	10	10	26	72	0.066350	0.068580	3.25
2	HSS	10	10	26	72	0.065160	0.0676546	3.69
4	HSS	16	19	32	92	0.012426	0.013230	6.08
3	HSS	16	19	32	92	0.011415	0.012325	7.38

2	HSS	16	19	32	92	0.010901	0.011842	7.94
4	Carbide	10	10	22	72	0.022255	0.022832	2.54
3	Carbide	10	10	22	72	0.021545	0.022216	3.02
2	Carbide	10	10	22	72	0.021307	0.022087	3.53
4	Carbide	16	16	32	92	0.007281	0.007580	3.94
3	Carbide	16	16	32	92	0.006950	0.007315	4.99
2	Carbide	16	16	32	92	0.006777	0.007163	5.38
4	Carbide	20	20	38	204	0.004368	0.004630	5.66
3	Carbide	20	20	38	104	0.004138	0.004463	7.27
2	Carbide	20	20	38	104	0.004062	0.004409	7.86

Table 4.2: Results of the analytic equations and ANSYS analysis

4.2.1.3. Simplified Equations for Tool Deflection

Modeling and FEA can be impractical and time consuming for each tool configuration in a virtual machining environment. Therefore, simplified equations are created to predict deflections of tools for given geometric parameters and material properties (elastic modulus and density). The static characteristics of end mills can be easily determined by these analytical expressions. After the comparison of analytical and FEA results, the corrected deflection equations are obtained by using MINITAB statistics.These equations has the following form:

$$Y = C.Y^{N} \quad analytic$$

$$C = \begin{cases} 0.984 & for \;\; 4-Flute \\ 0.985 & for \;\; 3-Flute \\ 0.983 & for \;\; 2-Flute \end{cases}$$

$$N = \begin{cases} 0.983 & for \;\; 4-Flute \\ 0.981 & for \;\; 3-Flute \\ 0.980 & for \;\; 2-Flute \end{cases} \qquad (4.16)$$

where $Y_{analytic}$ is in mm. The error in this approximation is less than % 1.

In the analytical deformation equations, the evaluation of the integral formulas is very complex. In an attempt to further simplify the deflection calculation, the following analysis is performed. The maximum deflection could be determined using

$$deflection_{\max} = C.\frac{F}{E}\left[\frac{L1^3}{D1^4} + \frac{(L2^3 - L1^3)}{D2^4}\right]^N$$

$$C = \begin{cases} 9.05 & for\ \ 4-Flute \\ 8.30 & for\ \ 3-Flute \\ 7.93 & for\ \ 2-Flute \end{cases} \qquad (4.17)$$

$$N = \begin{cases} 0.950 & for\ \ 4-Flute \\ 0.965 & for\ \ 3-Flute \\ 0.974 & for\ \ 2-Flute \end{cases}$$

where F (N) is the applied force and E (MPa) is the modulus of elasticity of the tool material. The geometric properties of the end mill are in mm. The error in this approximation is less than % 5.

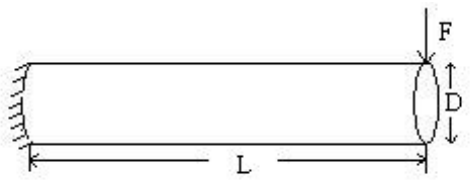

Figure 4.9: Boundary and loading conditions of the cylinder

If the shape of the end mill is assumed to be a cylinder, the stiffness of the tool will be very different from the stiffness obtained from simplified equations (Table 4.3). Figure 4.9 shows boundary and loading conditions of a cylinder. The stiffness of the cylinder is calculated by using cantilever beam method. [Beer and Johnston, 1992]

$$y_{\max} = \frac{FL^3}{3EI} = \frac{FL^3}{3E\frac{\pi D^4}{64}} \rightarrow k = \frac{F}{y_{\max}} = \frac{3E\pi D^4}{64L^3} \tag{4.18}$$

where k is the stiffness (N/mm). Diameter (D) and length (L) of the cylinder are in mm and elastic modulus (E) is in MPa (N/mm2)

Flute	Material	D1(mm)	D2(mm)	L1(mm)	L2(mm)	k-equation (N/mm)	k-cylinder (N/mm)
4	HSS	6	6	13	57	201	206
3	HSS	6	6	13	57	204	
2	HSS	6	6	13	57	205	
4	HSS	10	10	22	72	743	789
3	HSS	10	10	22	72	767	
2	HSS	10	10	22	72	776	
4	Carbide	10	10	22	72	2246	2387
3	Carbide	10	10	22	72	2321	
2	Carbide	10	10	22	72	2347	
4	Carbide	16	16	32	92	6867	7498
3	Carbide	16	16	32	92	7194	
2	Carbide	16	16	32	92	7378	

Table 4.3: Comparison of the stiffness values obtained from simplified equations and cylinder model

4.2.2. Tool Holder

The static characteristics of HSK (HSK-40, HSK-50 and HSK-63) and CAT (CAT-40 and CAT-50) tool holders were analyzed in ANSYS. The material properties for tool holders are summarized in Table 3.4 (Aoyama and Inasaki, 2001). Examples of the finite element model used for HSK and CAT tool holders are shown in Figure 3.10.

Modulus of Elasticity (GPa)	Poisson's Ratio	Density(kg/ m^3)
206	0.3	7860

Table 4.4: Mechanical Properties of the Tool Holder Material

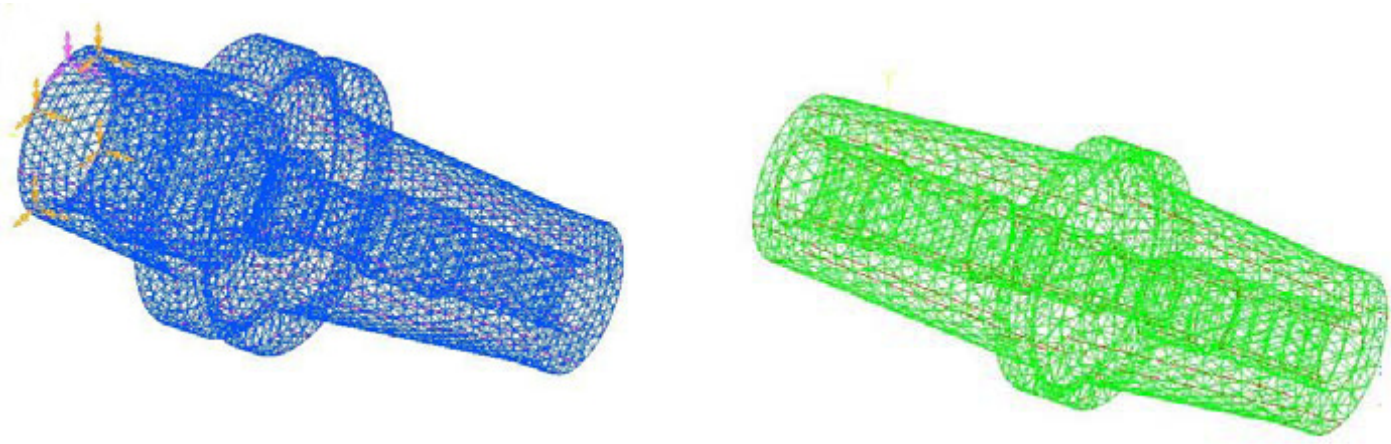

Figure 4.10: Example of FEM model for HSK and CAT tool holders

An example of deformation of the HSK type tool holder is shown in Figure 4.11. The displacement of tool holders and stiffness values are shown in Table 4.5.

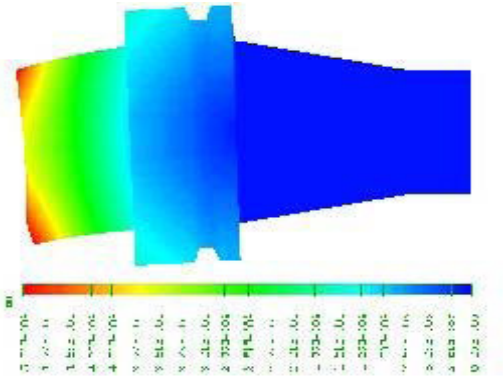

Figure 4.11: Example of deflection of a tool holder

Tool Holder Types	Max displacement (μm) Force=200N	Stiffness (KN/mm)
HSK-A40	1.38	24.60
HSK-A50	3.14	63.69
HSK-A63	9.02	22.17
CAT-40	3.53	56.66
CAT-50	4.26	46.95

Table 4.5: Results of ANSYS analysis of the tool holders

It can be concluded from Table 4.5 that the stiffness depends on the type of the tool holder.

4.3. Summary

In this chapter, geometric properties and material characteristics of tool and tool holder are explained. Models for end mill static deformations, which can be used for deflection calculations and surface form error, are presented. Generalized equations are developed to predictions stiffness for different tool geometry without measurement. The static characteristics of tool and tool holder are obtained using FEA analysis. FEA results are compared with analytical equation results.

CHAPTER FIVE
MODELING OF END MILL DYNAMICS

In this chapter, the dynamic analysis of milling tool and tool holder is presented. Dynamic properties play an important role in stability of machining process affecting part quality and productivity. Accurate knowledge of the machine dynamics is required for predicting dimensional accuracy. Frequency response function (FRF) measurements need to be performed to identify the dynamics of the systems experimentally. This can be very time consuming considering the number of tool-tool holder combinations in a production facility.

In the first section, a method for modeling dynamics of milling tool is presented. Some practical equations are developed to predict the dynamic properties of tools. Dynamic analysis of different geometry and material of the tool and tool holder, which are carried out by Finite Element Analysis (FEA) in ANSYS, are given in the second section. Considering great variety of cutting tool geometries, application of FEA to every case can be quite time consuming and unpractical. The results obtained from FEA and analytic dynamic equations are compared in the third section.

In the last section, the transfer function measurement and modal analysis are explained.

5.1. Dynamic Analysis of the Tool

5.1.1. Transverse Vibration of Bars

The differential equation of motion for the transverse vibration of beam can be derived from the deflection curve of discussed in strength of material.

This section briefly reviews the material necessary to make calculations of beam deflection and strain for an imposed load. The notation corresponds with the Figure (a). Recall for a linearly elastic beam that the strain in the x–direction, ε_x, is linearly related to the imposed normal stress in the x–direction, σ_x, by the following reaction(5.1)

$$\varepsilon_x = \frac{\sigma_x}{E} \tag{5.1}$$

where E is the modulus of elasticity.

In pure bending, the strain on a beam can be expressed in terms of the radius of curvature of the beam, R, and the distance from the neutral axis of the beam, y:

$$\varepsilon_x = -\frac{y}{R} \tag{5.2}$$

Hence, the strain is zero along the neutral axis and its magnitude increases with distance from the neutral axis. The strain is negative in the +y–direction, which corresponds to a negative stress or compression in the +y part of the beam. Equations (5.1) and (5.2) can be rearranged to give the stress at some position within the beam,

$$\sigma_x = -\frac{E_y}{R} \tag{5.3}$$

The moment, M(x), acting on the beam can be calculated from the stress:

$$M(x) = -\int_A y\sigma_x dA \tag{5.4}$$

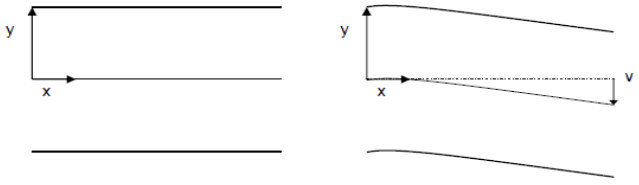

(a)

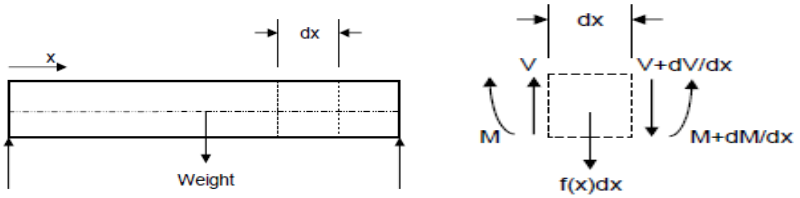

(b) Beam of uniform density

Force and moment balance within the beam

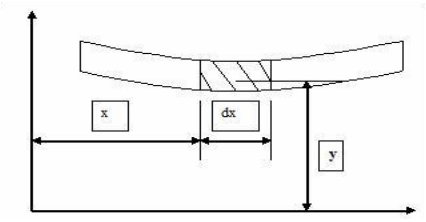

(c)

Figure 5.1 Free transverse vibration of beam with out external loading

Hence, a positive moment produces compression in the +y fibers of the beam.
Recalling the definition for the moment of inertia, I:

$$I = \int_A y^2 dA, \tag{5.5}$$

the moment-curvature relation can be found for a homogeneous beam:

$$M = \frac{EI}{R}, \tag{5.6}$$

and the flexure formula follows as:

$$\sigma_x = -\frac{M_y}{I} \tag{5.7}$$

The radius of curvature of the beam can be related to the displacement, v, of the neutral axis of the beam due to bending. For small deflections of the beam compared to the length of the beam, the radius of curvature can be determined from the following equation:

$$\frac{1}{R} = \frac{\frac{d^2v}{dx^2}}{[1+(\frac{d^2v}{dx^2})^2]^{3/2}} \tag{5.8}$$

This equation can be approximated as:

$$\frac{1}{R} = \frac{d^2v}{dx^2} \tag{5.9}$$

5.1.2 Analysis of beam vibration

Consider a beam of uniform cross section, A, and density, ρ, as shown in the

Figure (b). At some position x within the beam, a balance of forces and moments can be drawn using f(x) as some distributed load on the beam.

The resulting equations for the balance of the force and moments are as follows

(assuming that dx approaches zero):

$$-f(x) = \frac{dV}{dx} \tag{5.10}$$

And

$$V = \frac{dM}{dx} \tag{5.11}$$

These equations can be combined with the moment-deflection equation:

$$M = -EI\frac{\partial^2 v}{\partial x^2} \tag{5.12}$$

Note, here the deflection, v(x), is defined in the opposite sense as used in equation (5.2). These equations can be combined to give:

$$EI\frac{\partial^4 v}{\partial x^4} = f(x) \tag{5.13}$$

The distributed load is the inertial load due to vibration and can be represented as the product of the mass per unit length and the cross sectional area in the direction opposite of the acceleration:

$$f(x) = -\rho A\frac{\partial^2 v}{\partial t^2} \tag{5.14}$$

Combining equations (5.4) and (5.5) results in the following fourth order partial differential equation:

$$EI\frac{\partial^4 v}{\partial x^4} + \rho A\frac{\partial^2 v}{\partial t^2} = 0 \tag{5.15}$$

Where partial derivatives are used because v is a function of x and t. Since $a^2 = \frac{EI}{\rho A}$ equation (5.15) becomes

$$\frac{\partial^2 v}{\partial t^2} + a^2\frac{\partial^4 v}{\partial x^4} = 0 \tag{5.16}$$

The solution to this partial differential equation (5.16) is obtained by the standard method of variable separable.

i.e v(x, t) =X(x)T(t) (5.17)

substituting equation (5.17) in equation (5.16)

$$X\ddot{T} + a^2 X^{iv}T = 0$$

$$\frac{X^{iv}}{X} = -\frac{\ddot{T}}{a^2 T} \tag{5.18}$$

Since the left hand side is a function of x only and right hand side is a function of t only, it is logical to conclude each side should be constant.

Let this constant be p^2

$$a^2 \frac{X^{iv}}{X} = p^2$$
$$X^{iv} - \frac{p^2}{a^2} X = 0 \tag{5.19}$$

and

$$-\frac{\ddot{T}}{T} = p^2$$
$$\ddot{T} + p^2 T = 0 \tag{5.20}$$

Then we know the solution for equation (5.19and20)

$$T(t) = A\cos pt + B\sin pt$$
$$X(x) = C_1 \cos Rx + C_2 \sin Rx + C_3 \cosh Rx + C_4 \sinh Rx \tag{5.21}$$

where A, B, C_1, C_2, C_3, C_4 arbitrary constants and $R^4 = \frac{p^2}{a^2}$

since x is a function of space co-ordinates only, it is called normal function depicting the mode shape.

Hence the general solution to the partial differential equation (5.16) is written based on mathematics as:

$$v(x,t) = \sum_{i=1,2...} (A_i \cos p_i t + B_i \sin p_i t).(C_i \cos\sqrt{\frac{p_i}{a}}x + D_i \sin\sqrt{\frac{p_i}{a}}x + E_i \cosh\sqrt{\frac{p_i}{a}}x + F_i \sinh\sqrt{\frac{p_i}{a}}x)$$

(5.22)

where $A_i, B_i, C_i, D_i, E_i, F_i$ are arbitrary constants to be determined by the initial and boundary conditions. And p_i is the natural frequency.

5.1.3 Segmented Beam Model for Tool Dynamics

Dynamic analysis is used to determine mode shapes and natural frequencies of the cutting tool structures. A modeling method for transverse vibrations of an end mill is developed. End mill is a segmented beam, one segment for the part with flute and the other segment for the shank. The beam model with two different geometric segments is shown in Figure 5.1. Dynamic analysis of segmented beam has been carried as it was not available in the vibration literature.

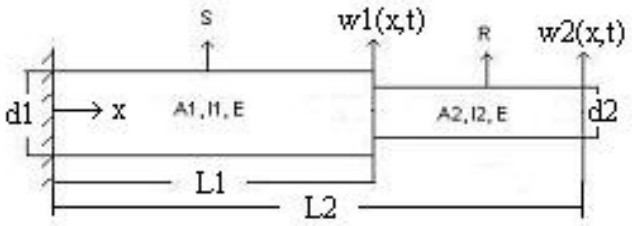

Figure 5.2 The geometry of the beam with two different geometric segments

I1, I2 and A1, A2 are the moment of inertias and the areas of the segments, respectively. R(x) and S(y) are the mode shapes, and w1 (x, t), and w2 (x, t) are the displacement functions.

For a slender beam with two different geometric segments, the associated displacement functions w1 (x, t), and w2 (x, t) can be written in the following form;

$$\begin{aligned} w1(x,t) &= S(x).e^{i\omega t} \qquad ,0 \le x \le L1 \\ w2(x,t) &= R(x).e^{i\omega t} \qquad ,L1 \le x \le L2 \end{aligned} \tag{5.23}$$

The governing equations of motion, neglecting the rotational inertia and shear formation, can be converted into the well-known Euler-Bernoulli equations [Chaudhari and Maiti, 2000]:

$$\begin{aligned} EI1\frac{d^4S}{dx^4} - \rho A1\omega^2 S = 0 \qquad &,0 \le x \le L1 \\ EI2\frac{d^4R}{dx^4} - \rho A2\omega R = 0 \qquad &,L1 \le x \le L2 \end{aligned} \tag{5.24}$$

where E is the modulus of elasticity and ρ is the density. The solution of equation (5.24) can be expressed as [Rao, 1995]

$$R(x) = A1.\cosh(\beta x) + A2.\sinh(\beta x) + A3.\cos(\beta x) + A4.\sin(\beta x)$$
$$S(x) = A5.\cosh(\alpha x) + A6.\sinh(\alpha x) + A7.\cos(\alpha x) + A8.\sin(\alpha x) \tag{5.25}$$

moment and shear force where A1, A2, A3, A4, A5, A6, A7 and A8 are arbitrary constants. It is necessary to accompany the general solutions with the boundary conditions. The boundary conditions are as follows. At *x=L2* (i.e. at the free end), bending must vanish:

$$EI2\frac{d^2R(L2)}{dx^2} = 0 \rightarrow \frac{d^2R(L2)}{dx^2} = 0$$
$$A1\cosh(\beta L2) + A2\sinh(\beta L2) - A3\cos(\beta L2) - A4\sin(\beta L2) \tag{5.26}$$

$$\frac{d}{dx}EI2\left(\frac{d^2R(L2)}{dx^2}\right) = 0 \rightarrow \frac{d^3R(L2)}{dx^3} = 0$$
$$A1\sinh(\beta L2) + A2\cosh(\beta L2) + A3\sin(\beta L2) - A4\cos(\beta L2) = 0 \tag{5.27}$$

At *x=L1* the continuity equations for displacement, slope, moment and shear force are as follows:

$$R(L1) = S(L1)$$
$$A1\cosh(\beta L1) + A2\sinh(\beta L1) + A3\cos(\beta L1) + A4\sin(\beta L1) -$$
$$A5\cosh(\alpha L1) - A6\sinh(\alpha L1) - A7\cos(\alpha L1) - A4\sin(\alpha L1) = 0 \tag{5.28}$$

$$\frac{dR(L1)}{dx} = \frac{dS(L1)}{dx}$$
$$A1\sinh(\beta L1) + A2\cosh(\beta L1) - A3\sin(\beta L1) + A4\cos(\beta L1) -$$
$$\frac{\alpha}{\beta}A5\sinh(\alpha L1) - \frac{\alpha}{\beta}A6\cosh(\alpha L1) + \frac{\alpha}{\beta}A7\sin(\alpha L1) - \frac{\alpha}{\beta}A8\cos(\alpha L1) = 0 \tag{5.29}$$

$$\frac{d^2R(L1)}{dx^2} = \frac{d^2S(L1)}{dx^2}$$

$$A1\cosh(\beta L1) + A2\sinh(\beta L1) - A3\cos(\beta L1) - A4\sin(\beta L1) - \left(\frac{\alpha}{\beta}\right)^2 A5\cosh(\alpha L1) - \left(\frac{\alpha}{\beta}\right)^2 A6\sinh(\alpha L1) + \left(\frac{\alpha}{\beta}\right)^2 A7\cos(\alpha L1) + \left(\frac{\alpha}{\beta}\right)^2 A8\sin(\alpha L1) = 0 \quad (5.30)$$

$$\frac{d^3R(L1)}{dx^3} = \frac{d^3S(0)}{dy^3}$$

$$A1\sinh(\beta L1) + A2\cosh(\beta L1) + A3\sin(\beta L1) - A4\cos(\beta L1) - \left(\frac{\alpha}{\beta}\right)^3 A5\sinh(\alpha L1) - \left(\frac{\alpha}{\beta}\right)^3 A6\cosh(\alpha L1) - \left(\frac{\alpha}{\beta}\right)^3 A7\sin(\alpha L1) + \left(\frac{\alpha}{\beta}\right)^3 A8\cos(\alpha L1) = 0 \quad (5.31)$$

At *x=0* (i.e. at the fixed end) displacement and slope are zero:

$$S(0) = 0$$
$$A5 + A7 = 0 \quad (5.32)$$

$$\frac{dS(0)}{dx} = 0$$
$$A6 + A8 = 0 \quad (5.33)$$

These 8 conditions defined by equations (5.26 - 5.33) are sufficient to solve for the 8 arbitrary constants. The equations involving these constants can be written in the following form

$$[C]\{A\} = 0 \quad (5.34)$$

where A_j is the vector of the 8 arbitrary constants and the coefficient matrix [C] is of dimension (8 x 8), and is given by

$$[C]=\begin{bmatrix}
\cosh(\beta 2) & \sinh(\beta 2) & -\cos(\beta 2) & -\sin(\beta 2) & 0 & 0 & 0 & 0 \\
\sinh(\beta 2) & \cosh(\beta 2) & \sin(\beta 2) & -\cos(\beta 2) & 0 & 0 & 0 & 0 \\
\cosh(\beta 1) & \sinh(\beta 1) & \cos(\beta 1) & \sin(\beta 1) & -\cosh(\alpha 1) & -\sinh(\alpha 1) & -\cos(\alpha 1) & -\sin(\alpha 1) \\
\sinh(\beta 1) & \cosh(\beta 1) & -\sin(\beta 1) & \cos(\beta 1) & -\frac{\alpha}{\beta}\sinh(\alpha 1) & -\frac{\alpha}{\beta}\cosh(\alpha 1) & \frac{\alpha}{\beta}\sin(\alpha 1) & -\frac{\alpha}{\beta}\cos(\alpha 1) \\
\cosh(\beta 1) & \sinh(\beta 1) & -\cos(\beta 1) & -\sin(\beta 1) & -\frac{\alpha^2}{\beta^2}\cosh(\alpha 1) & -\frac{\alpha^2}{\beta^2}\sinh(\alpha 1) & \frac{\alpha^2}{\beta^2}\cos(\alpha 1) & \frac{\alpha^2}{\beta^2}\sin(\alpha 1) \\
\sinh(\beta 1) & \cosh(\beta 1) & \sin(\beta 1) & -\cos(\beta 1) & -\frac{\alpha^3}{\beta^3}\sinh(\alpha 1) & -\frac{\alpha^3}{\beta^3}\cosh(\alpha 1) & -\frac{\alpha^3}{\beta^3}\sin(\alpha 1) & \frac{\alpha^3}{\beta^3}\cos(\alpha 1) \\
0 & 0 & 0 & 0 & 1 & 0 & 1 & 0 \\
0 & 0 & 0 & 0 & 0 & 1 & 0 & 1
\end{bmatrix}$$

(5.35)

The characteristic equation is determined when determinant of the coefficient matrix C (5.35) is equal to zero. In order to write of the characteristic equation with one unknown, the ratio between β and α values is calculated by using the frequency equation, which is derived from equation 5.24.

$$\frac{d^4S}{dx^4}-\frac{\rho A1}{EI1}\omega^2 S=0\rightarrow\frac{d^4S}{dx^4}-\alpha^4\omega^2 S=0\rightarrow\omega=\alpha\sqrt{\frac{EI1}{\rho A1}}$$
$$\frac{d^4R}{dx^4}-\frac{\rho A2}{EI2}\omega^2 R=0\rightarrow\frac{d^4R}{dx^4}-\beta^4\omega^2 R=0\rightarrow\omega=\beta^2\sqrt{\frac{EI2}{\rho A2}} \qquad (5.36)$$
$$\omega^2=\alpha^2\sqrt{\frac{EI1}{\rho A1}}=\beta^2\sqrt{\frac{EI2}{\rho A2}}\rightarrow\frac{\beta^2}{\alpha^2}=\sqrt{\frac{I2A1}{A2I1}}\rightarrow\frac{\beta}{\alpha}=\sqrt{\frac{d2}{d1}}$$

The simple form of matrix (5.35) is obtained by using $\frac{L1}{L2}(I)$ and $\sqrt{\frac{d2}{d1}}(d)$ ratios. There is only one unknown, x ($\beta L2$) in this form.

$$[C]=\begin{bmatrix}
\cosh(x) & \sinh(x) & -\cos(x) & -\sin(x) & 0 & 0 & 0 & 0 \\
\sinh(x) & \cosh(x) & \sin(x) & -\cos(x) & 0 & 0 & 0 & 0 \\
\cosh(xl) & \sinh(xl) & \cos(xl) & \sin(xl) & -\cosh(x\frac{l}{d}) & -\sinh(x\frac{l}{d}) & -\cos(x\frac{l}{d}) & -\sin(x\frac{l}{d}) \\
\sinh(xl) & \cosh(xl) & -\sin(xl) & \cos(xl) & -\frac{1}{d}\sinh(x\frac{l}{d}) & -\frac{1}{d}\cosh(x\frac{l}{d}) & \frac{1}{d}\sin(x\frac{l}{d}) & -\frac{1}{d}\cos(x\frac{l}{d}) \\
\cosh(xl) & \sinh(xl) & -\cos(xl) & -\sin(xl) & -\frac{1}{d^2}\cosh(x\frac{l}{d}) & -\frac{l}{d^2}\sinh(x\frac{l}{d}) & \frac{1}{d^2}\cos(x\frac{l}{d}) & \frac{1}{d^2}\sin(x\frac{l}{d}) \\
\sinh(xl) & \cosh(xl) & \sin(xl) & -\cos(xl) & -\frac{1}{d^3}\sinh(x\frac{l}{d}) & -\frac{1}{d^3}\cosh(x\frac{l}{d}) & -\frac{1}{d^3}\sin(x\frac{l}{d}) & \frac{1}{d^3}\cos(x\frac{l}{d}) \\
0 & 0 & 0 & 0 & 1 & 0 & 1 & 0 \\
0 & 0 & 0 & 0 & 0 & 1 & 0 & 1
\end{bmatrix} \quad (5.37)$$

βL2 or αL1 values are computed from characteristic equation, i.e. determinant of the coefficient matrix C (5.37) for different modes. For any beam, there will be an infinite number of normal modes with one natural frequency associated with each normal mode. The natural frequencies of segmented beam

$$\omega = (\alpha L1)^2 \sqrt{\frac{EI1}{\rho A1 L1^4}} \qquad or \qquad \omega = (\beta L2)^2 \sqrt{\frac{EI2}{\rho A2 L2^4}} \qquad (5.38)$$

After determining the coefficient matrix *C*, arbitrary constants vector *A* can be computed from equation (5.34). The mode shapes *R (x)* and *S (y)* (equation 5.25) according to the frequencies are obtained by using *A1*, *A2*, *A3*, *A4*, *A5*, *A6*, *A7* and *A8*.

5.1.4. Simplified Equations for Natural Frequencies and Mode Shapes

Segmented beam model was used to determine cutting tool dynamics. This beam model can be used in many areas. However, the calculations of the natural frequencies and mode shapes are very difficult because of the complex coefficient matrix (5.35). Simplified equations are developed to calculate the solution of the characteristic equation easily. The solution of the determinant of the complex coefficient matrix can be repeated for various

segmented beam geometries. The natural frequency equations of segmented beam (5.38) can be rewritten in the following form:

$$\omega = (\alpha L1)^2 \sqrt{\frac{EI1}{\rho A1 L1^4}} \qquad or \qquad \omega = (\beta L2)^2 \sqrt{\frac{EI2}{\rho A2 L2^4}}$$
$$\omega = K \sqrt{\frac{EI1}{\rho A1 L1^4}} = \left(K \frac{d1}{d2} \frac{L2^2}{L1^2} \right) \sqrt{\frac{EI2}{\rho A2 L2^4}} \tag{5.39}$$

In derivation of the equations to determine *K*, the length ratio (*L1/L2*) and the diameter ratio (*D1/D2*) are used. Therefore, the *K* value can be calculated for any given geometric properties. The graph for the variation in the *K* value for first mode according to *L1/L2* and *D1/D2* ratio is shown in Figure 5.2.

In Figure 5.2, the relation between *1/K* and *D1/D2* is linear. The slope and the constant of the line change according to *L1/L2* ratio. In order to calculate the natural frequency of the first mode, the equation between *K* and geometric properties is derived

$$\frac{1}{K} = a\left(\frac{D1}{D2}\right) + b \rightarrow K = \frac{1}{a\left(\frac{D1}{D2}\right) + b} \tag{5.40}$$

Where

$$a = \frac{-0.817(\ln l) + 0.0167}{l}$$
$$b = 0.1821 l^2 + 0.1063 l - 0.0275$$
$$l = \frac{L1}{L2}$$

The graph given in Figure 5.3, or equation 5.40, can be used to determine K based on L1/L2 and D1/D2 for any segmented beam with two sections.

Then, the fundamental natural frequency can be determined from equation 5.39 eliminating the need for eigenvalue solution for matrix (5.35). Therefore, the fundamental frequency of a segmented beam can be determined analytically, which is an original contribution.

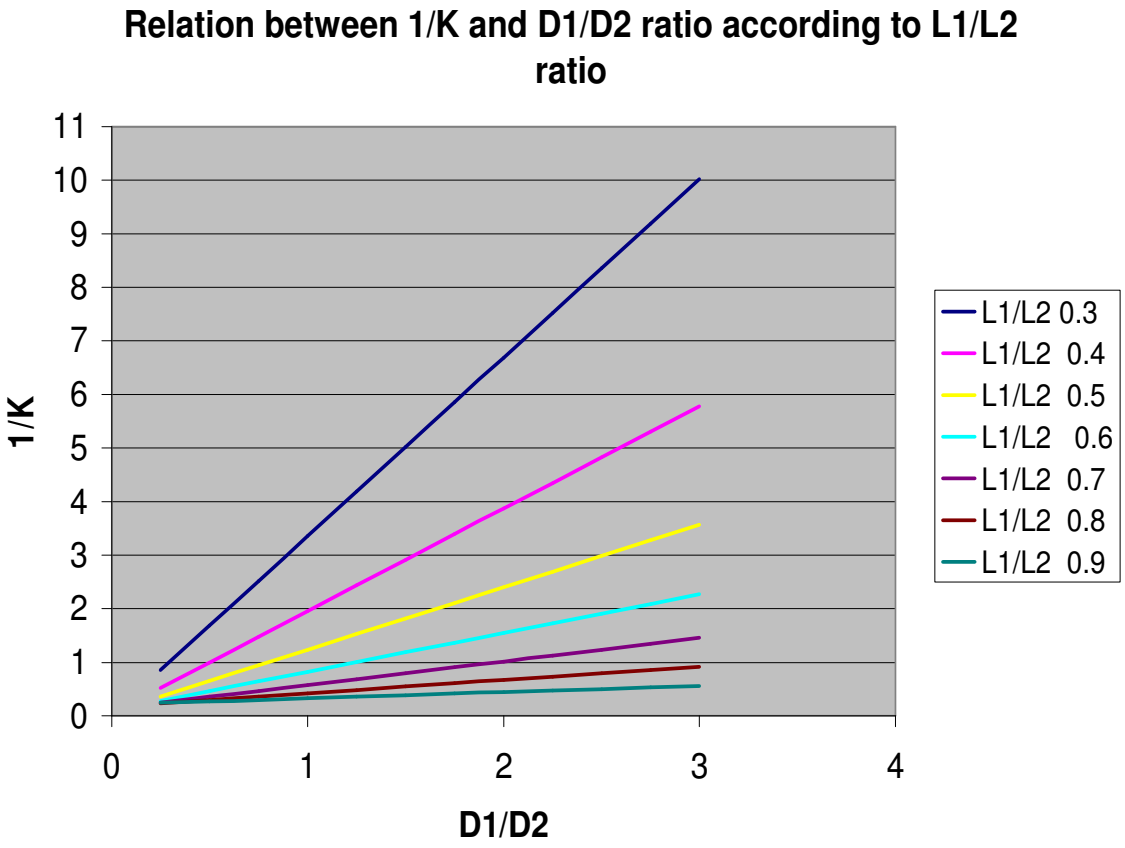

Figure 5.3: Relation between 1/K and D1/D2 ratio according to L1/L2 ratio

5.2. Modeling and FEA Analysis

In ANSYS, models are built to define geometry, material properties, element types and constraints for end mills. Natural frequencies and mode shapes are obtained using FEA. [Shih, 2000]

5.2.1. Tool

Many end mills with different material and geometric parameters are analyzed. As an example, natural frequencies and mode shapes of a HSS end mill with 4-Flute, 16 mm diameter and 92 mm length are shown in Figure 5.3.

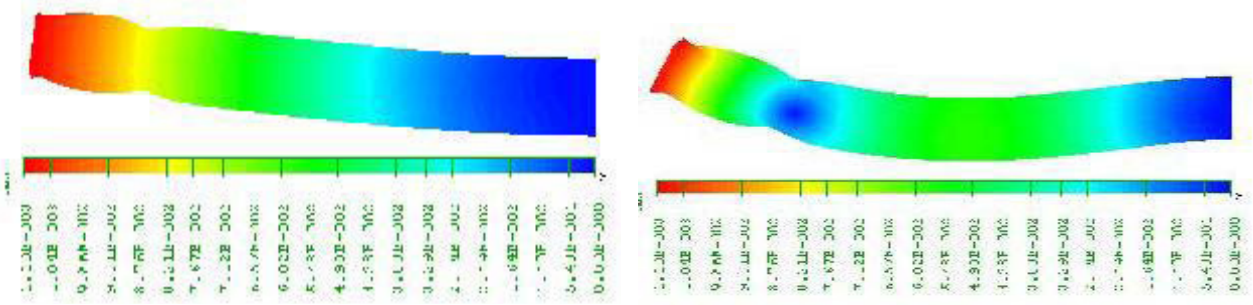

Mode1: 1476 Hz

Mode2: 7134 Hz

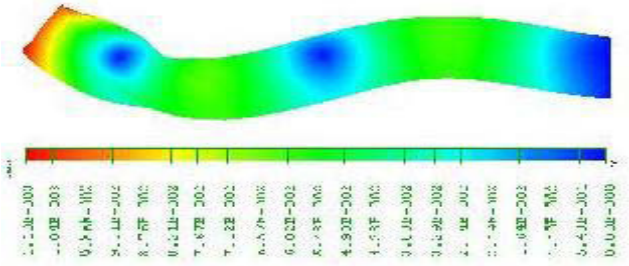

Mode3: 16764 Hz

Figure 5.4: Example of natural frequencies and mode shapes of a tool

The natural frequencies of HSS tools according to geometric properties of the end mill and frequency description are given in Table 5.2. The lateral and vertical bending frequencies are different for 2-flute cutter. The cross section of the 2-flute cutter is not symmetric with respect to x and y-axes, so the moment of inertia I_{xx} and I_{yy} are different.

Frequency(Hz)		D_1=6mm, L_1=13mm L_2=57mm D_2=6mm			D_1=10mm, L_1=22mm L_2=72mm D_2=10mm			D_1=16mm, L_1=31mm L_2=92mm D_2=16mm			D_1=20mm, L_1=38mm L_2=104mm D_2=20mm		
DESCRIPTION	TYPE	4 Flute	3 Flute	2 Flute	4 Flute	3 Flute	2 Flute	4 Flute	3 Flute	2 Flute	4 Flute	3 Flute	2 Flute
First Bending	**X**	1409	1500	1435	1504	1620	1534	1476	1600	1505	1443	1565	1468
First Bending	**Y**	1409	1500	1437	1504	1620	1539	1476	1600	1516	1443	1565	1483
Second Bending	**X**	7890	8072	7846	7755	7662	7475	7134	6897	6729	6800	6477	6328
Second Bending	**Y**	7890	8072	8005	7755	7662	7918	7134	6897	7331	6800	6477	6969
Third Bending	**X**	19604	18939	18623	18543	19218	18643	16764	15918	15671	15798	15009	14782
Third Bending	**Y**	19604	18939	19992	18543	19218	19018	16764	15918	17218	15798	15009	16214

Table 5.1: Natural frequencies (ANSYS) of HSS end mills with different geometry

As the tool length/diameter ratio increases, the natural frequency of the tool decreases (Figure 5.4). 2-flute cutters have the greatest natural frequency and 4-flute cutters have the least because of the cross section. The natural frequencies of the cylinder that has the same diameter and length with other tools are also calculated. This graph shows that considering the tool as a cylinder is a bad approximation.

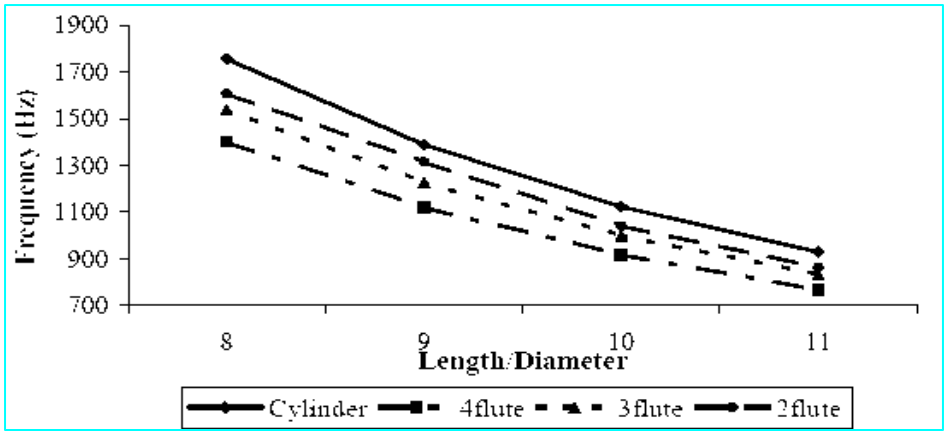

Figure 5.5: Relationship between natural frequencies (Mode1) of HSS tool and tool length/ diameter ratio

Frequency(Hz)		D_1=6mm, L_1=13mm L_2=57mm D_2=6mm			D_1=10mm, L_1=22mm L_2=72mm D_2=10mm			D_1=16mm, L_1=31mm L_2=92mm D_2=16mm			D_1=20mm, L_1=38mm L_2=104mm D_2=20mm		
DESCRIPTION	TYPE	4 Flute	3 Flute	2 Flute	4 Flute	3 Flute	2 Flute	4 Flute	3 Flute	2 Flute	4 Flute	3 Flute	2 Flute
First Bending	**X**	2033	2164	2069	2169	2340	2210	2129	2309	2154	2082	2258	2118
First Bending	**Y**	2033	2164	2069	2169	2340	2210	2129	2309	2154	2082	2258	2118
Second Bending	**X**	11381	11646	11033	11187	11081	10922	10291	9950	10026	9765	9343	9033
Second Bending	**Y**	11381	11646	11549	11187	11081	11432	10291	9950	10026	9765	9343	10054
Third Bending	**X**	28282	27322	27624	26750	27727	26238	24189	22968	23657	22791	21655	22185
Third Bending	**Y**	28282	27322	28841	26750	27727	27436	24189	22968	24838	22971	21655	23391

Table 5.2: Natural frequencies (ANSYS) of carbide end mills with different geometry

The lateral and vertical bending frequencies of carbide tools according to geometric properties and frequency description are given in Table 5.2. The carbide tools have higher natural frequency than HSS tools because of their high modulus of elasticity (Figure 5.6)

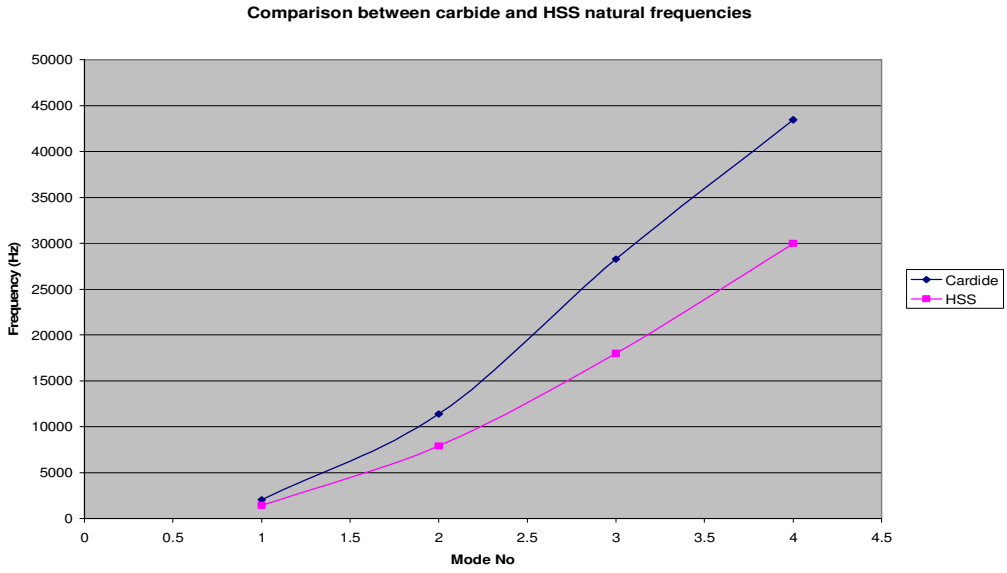

Figure 5.6: Comparison between carbide and HSS natural frequencies

5.3 Tool Holder

The dynamic characteristics of HSK (HSK-40, HSK-50 and HSK-63) and CAT (CAT-40 and CAT-50) tool holders were analyzed in ANSYS. The first and second natural frequencies of tool holders are summarized in Table 5.3.

	First Bending (kHz)		Second Bending (kHz)	
Tool Holder Type	Lateral	Vertical	Lateral	Vertical
HSK-A40	14.74	14.74	20.50	20.70
HSK-A50	13.66	13.67	31.61	31.61
HSK-A63	13.85	13.87	28.48	28.56
CAT-40	8.05	8.06	22.73	22.73
CAT-50	7.19	7.19	21.70	21.71

Table 5.3: Results of the FEA for the tool holders in ANSYS

5.3.1. Comparison of the Results from Finite Element Analysis and Analytic Solution

Analytic equations, which are used to predict dynamic behavior of the cutting tools, are compared with ANSYS finite element analysis. Table 4.4 shows the error between the ANSYS FE and analytic solution for 4-flute HSS end mill, which has 6 mm flute diameter, 13 mm flute length, 57 overall length and 6 mm in shank diameter. From Table 4.4, the error between FEM frequency and analytic calculated frequency increases from % 5 for mode1 to % 18 for mode 3.

4-FLUTE	**Frequency-Analytic(Hz)**	**Frequency-ANSYS(Hz)**	**ERROR (%)**
First Bending	1409	1476	**4.74**
Second Bending	7890	8530	**8.12**
Third Bending	19601	23170	**18.21**

Table 5.4: Comparison of the natural frequencies of FE and analytic analysis

Table 5.5 shows the displacement errors between the ANSYS FE and analytic analysis for the fist three modes. The mode shapes representations, which are drawn using analytic equations, are given in Table 5.5 for three modes of the 4-flute cutting tool. Critical displacements values and their positions along the tool length are compared. The error in maximum displacement is in the range of % 3.5 - %12.5. As tool diameter and tool length increases, the error in the natural frequencies between FEM and analytic model

4-Flute(ANSYS)		**ANALYTIC**		
x/L	**Displacement(mm)**	**x/L**	**Displacement(mm)**	**ERROR (%)**
0	0.0000	**0**	0.0000	**-**
1/4	0.1138	**1/4**	0.1147	**0.79**
2/4	0.4100	**2/4**	0.3943	**3.83**
3/4	0.7860	**3/4**	0.7541	**4.06**
1	1.1770	**1**	1.1365	**3.44**

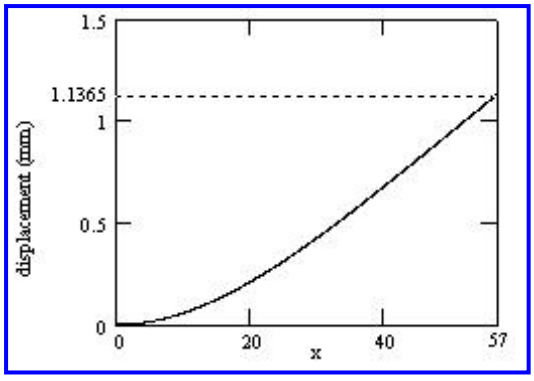

a) Mode 1

4-Flute(ANSYS)		ANALYSIS		
x/L	Displacement(mm)	x/L	Displacement(mm)	ERROR (%)
0	0.0000	**0**	0.0000	-
A/L=0,456	0.7403	**A/L=0.7738**	0.7738	4.52
B/L=0,761	0.0000	**B/L=0,742**	0.0000	-
C/L=1	1.3450	**C/L=1**	1.4301	**6.33**

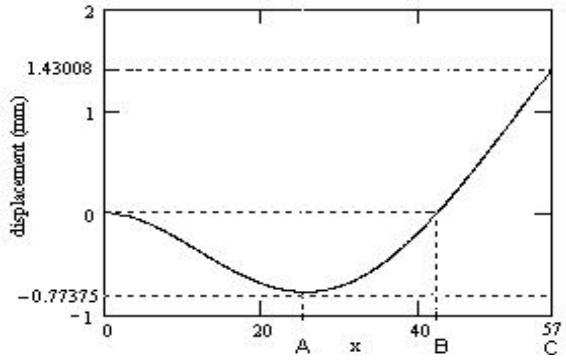

b) Mode 2

4-Flute(ANSYS)		ANALYSIS		
x/L	Displacement(mm)	x/L	Displacement(mm)	ERROR (%)
0	0.0000	0	0.0000	-
A/L=0,283	0.6490	A/L=0,282	0.6509	0.30
B/L=0,5	0.0000	B/L=0,488	0.0000	-
C/L=0,7	0.5870	C/L=0,672	0.5655	3.66
D/L=0,867	0.0000	D/L=0,842	0.0000	-
E/L=1	1.2360	E/L=1	1.0827	12.40

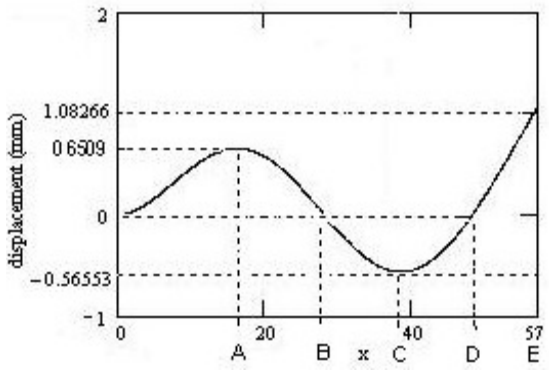

c) Mode 3

Table 5.5: Comparison of the mode shapes of FE and analytic analysis

5.4. Summary

In this chapter, a method of modeling for transverse vibrations of geometrically segmented beam is proposed. End mill is assumed to be as segmented beam with one end fixed and other end free. In order to obtain natural frequency and mode shape of the system, complex matrix calculations are needed. Simplified equations are derived to eliminate time consuming calculations. In these equations, desired geometric properties can be selected for prediction.

Finite Element Analysis (FEA) results of various tool geometries, different materials and tool holder types are given. These results are compared with the results obtained from analytic equations.

CHAPTER SIX

MODELING OF STABLITY LOBE DIAGRAM

6.1 Creating a Stability Lobe Diagram

In this chapter we have focused on topics such as multimode chattering, variations of machine tools and cutting tools, numerical modeling, and instrumental measurements. However, a thorough discussion of chatter theory and equations, along with improvement to techniques for creating the stability lobe diagram, are equally important. In particular, they are valuable in the classroom, so that students can easily create a stability lobe diagram and practice optimizing cutting parameters. Manufacturing industries can also apply the theory by using practical and simplified techniques to improve MRR and production rate. A method is presented below to create the stability lobe diagram using a spreadsheet. It also presents an analytical rather than graphical method of calculating the approximate optimal chip widths.

6.2. Governing equations of machine chattering

The governing equations of machine chattering can be derived from the general equation of vibration and the regenerative chatter equations.

6.2.1 Critical chip width

In orthogonal cutting, the cutting force F is proportional to the cutting area (the product of the chip width or depth of cut b and thickness h):

$$F = k_s\, b\, h = k_s\, b\, [x(t - T) - x(t)] \tag{6.1}$$

where k_s is the cutting stiffness or specific power, x is the displacement of the cutter normal to the cut, t is time, and T is the time interval between the previous and current cuts. Substituting equation (6.1) into the general equation of vibration:

$$m\ddot{x} + c\dot{x} + kx = F \tag{6.2}$$

We obtain the formula for chip width [4]:

$$b = \frac{-1}{2k_s G_R} \tag{6.3}$$

where G_R is the real part of the frequency response function (FRF) G as in the standard solution of equation (6.2) alone,

$$\frac{x}{F} = \frac{1-r^2}{k[(1-r^2)^2 + (2\zeta r)^2]} + i\frac{-2\zeta r}{k[(1-r^2)^2 + (2\zeta r)^2]} = G_R + iG_I = G \tag{6.4}$$

In equation (6.2, 6.3 and 6. 4):

m = Mass

c = Damping coefficient

k = Stiffness (k = F / x)

r = Ratio of chatter frequency to natural frequency (r = f / fn). The natural frequency fn of the machining system is also called the modal frequency.

ζ = Ratio of the damping coefficient to the critical damping coefficient $(\zeta = c/c_c)$. The critical damping coefficient $c_c = 2\sqrt{km}$.

When we solve equation (6.1) and equation (6.2) together, the chip width b is dependent on the frequency f of machine vibration or chatter through the frequency ratio r. For each chatter frequency generated on a machining system, there is a corresponding critical chip width b. The cutting process is stable when its chip width is less than the critical value and unstable otherwise.

6.2.2 Minimum chip width

The chip width b should always be positive (greater than or equal to zero.) Therefore, from equation (6.3) and equation (6.4), the minimum chip width $b_{\min}$ occurs at the maximum negative value of G_R (or true minimum $G_{R,\min,}$) when $r = \sqrt{1+2\zeta}$ [4]:

$$b_{\min} = \frac{-1}{2k_s G_{R,\min}} = \frac{2k\zeta(1+\zeta)}{k_s} \tag{6.5}$$

This minimum chip width represents a limit in a machining process. Since it is independent of the chatter frequency, there is only a fixed value determined by the materials and geometries of the cutter and the workpiece. A cutting process is

unconditionally stable when the chip widths are under this critical value. A dimensionless chip width may be represented by the ratio of chip width to the minimum chip width [5]:

$$r_b = \frac{b}{b_{\min}} = \frac{G_{R,\min}}{G_R} = \frac{(1-r^2)^2 + (2\zeta r)^2}{-4\zeta(1+\zeta)(1-r^2)} \tag{6.6}$$

Equation (6.3) represents the relationship between the chip width b and chatter frequency f ($f = rf_n$). While equation (6.6) represents the relationship between the dimensionless chip width ratio r_b and chatter frequency ratio r.

6.2.3 Equations of regenerative chatter

Roughness or waviness always exists on the machined surface of workpieces due to vibrations. According to regenerative chatter theory, chatter occurs whenever there is a shift of the phase angle ε between the current and previous surface waviness. Therefore, the ratio of chatter frequency f to tooth-stroke frequency f_t represents the number of surface waves between consecutive cutter teeth, and can be written as an integer n (also called the lobe number. n = 0, 1, 2, …) plus a fraction of ε / 2π radians[5]:

$$\frac{f}{f_t} = \frac{r}{r_t} = n + \frac{\varepsilon}{2\pi} \tag{6.7}$$

where r_t is the ratio between the tooth frequency and natural frequency ($r_t = f_t / f_n$). The phase shift angle ε between the current and previous surface waviness may be expressed as [5]:

$$\varepsilon = \pi + 2\tan^{-1}\frac{G_I}{G_R} \tag{6.8}$$

Since the real and imaginary FRF's G_R and G_I are both negative (equation6.4), using the principal range of $-\pi/2 < \tan^{-1} x < \pi/2$, we have $0 < \tan^{-1}(G_I / G_R) < \pi/2$, and the phase shift angle ε is between $\pi < \varepsilon < 2\pi$.

Substitute equation (6.3) into equation (6.8), and then into equation (6.7), we obtain the equation of regenerative chatter:

$$\frac{f}{f_t} = \frac{r}{r_t} = n + \frac{1}{2} + \frac{1}{\pi}\tan^{-1}\frac{-2\zeta r}{1-r^2} \tag{6.9}$$

Equation (6.9) represents the relationships among the chatter frequency f (or r), the tooth frequency f_t (or r_t), and the lobe number n. Together with equation (6.3) (or

equation 6.6), they form the governing relationship between the chip width b and spindle speed N, or between the dimensionless chip width ratio r_b and chatter frequency ratio r_t. The spindle speed N can be related to the tooth frequency $f_t (f_t = n_t N / 60)$ where n_t is the number of teeth on the cutter. For multiple-teeth cutters and multiple degrees of freedom, additional parameters and equations are necessary. It has also been observed both theoretically and practically that the relationships represented by the machine chattering equations do not hold for machining processes with very low spindle speeds. Tobias and Fishwick [2] derived equations under different conditions in the low-speed range. These topics are beyond the scope of this thesis.

6.3. The stability lobe diagram

From equation (6.3) and equation (6.9), we can create a stability lobe diagram between the chip width b and spindle speed N (Figure 1). We may also create a stability lobe diagram between the dimensionless $r_b = b / b_{\min}$ and $r_t = f / f_t$ from equation (6.6) and equation (6.9) (Figure 2). The dimensionless stability lobe diagram has the advantage of allowing comparisons among different machining conditions. Mixed dimensions are also possible, such as b ~ r_t and r_b ~ N, but not recommended.

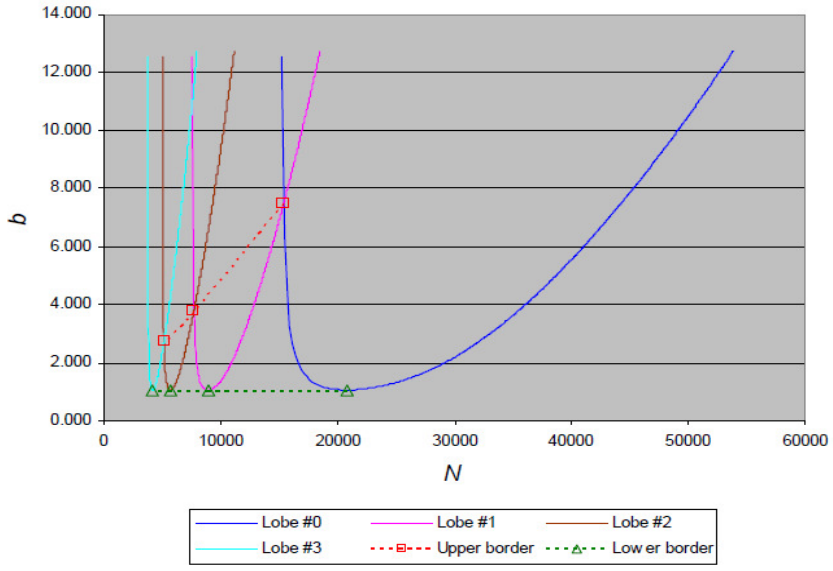

Figure 6.1 Stability lobe diagram for the prediction of the maximum chip width

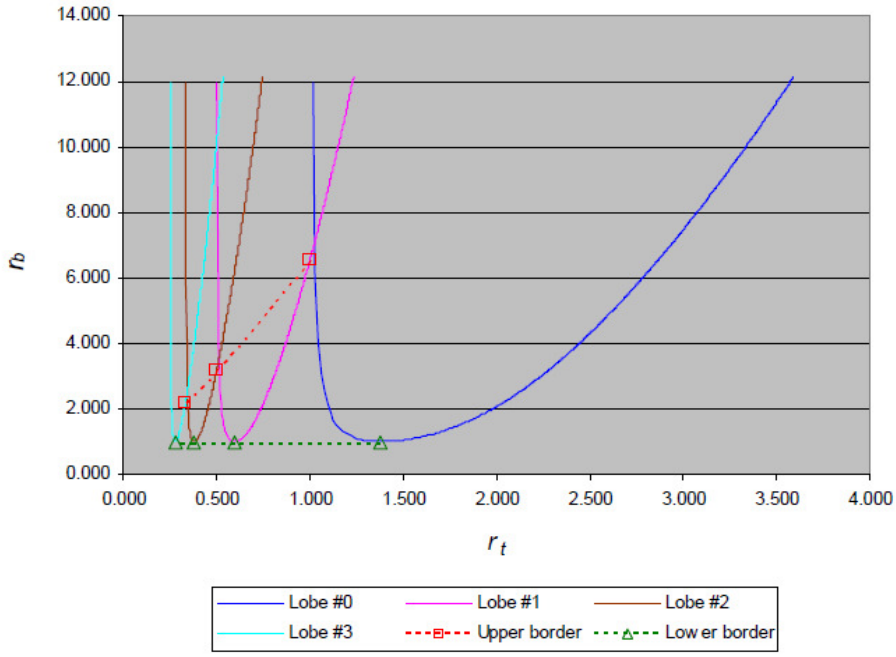

Figure 6.2 Stability lobe diagram (dimensionless)

Since the series of relationship curves in Figure 6.1 and Figure 6.2 are shaped like lobes, the graph is usually called a stability lobe diagram. A stability lobe diagram shows the relationship between chip width (or depth of cut) and spindle speed, with the lobe number as a parameter. Usually, the variable on its x-axis is represented as spindle speed N, tooth frequency $f_t (f_t = n_t N / 60)$, or the tooth frequency ratio $r_t (r_t = f_t / f_n)$; the variable on its y-axis is represented as chip width b or the chip width ratio $r_b (r_b = b / b_{\min})$. The dimensionless relationship of $r_b \sim r_t$ will be discussed. The lobes and their characteristics are similar for the other variables.

It is more convenient to calculate the points on the lobes using spreadsheet software. The step-by- step procedure for generating the points is illustrated in Table6. 1.

j	f_j	r_j	r_{bj}	r_{tjn}				
				n=0	n=1	n=2	n=4	…
1	251	1.004	6.026	1.026	0.506	0.336	0.252	…
2	252	1.008	4.061	1.053	0.513	0.339	0.253	…
3	253	1.012	2.135	1.081	0.519	0.342	0.255	…
4	254	1.016	1.678	1.108	0.526	0.345	0.256	…
…	…	…	…	…	…	…	…	…

Table 6.1 Calculating the stability lobes of $r_b \sim r_t$

Step 1. For each increment j of the chatter frequency f_j, calculate r_j and r_{bj} from equation (6.6).

Step 2. For each lobe number n, calculate its corresponding r_{tjn} from equation (6.9).

Step 3. The points for each n value are plotted to form a single lobe, and a series of lobes (n = 0, 1, 2 …) are plotted to form the stability lobe diagram of $r_b \sim r_t$.

In Table 1, the subscript j indicates the chatter frequency f after the j^{th} increment. The procedure to create the stability lobes of b ~ N is the same as that of $r_b \sim r_t$, except that equation(6.3) is used to calculate b instead of using equation(6.6) to calculate r_b, and the spindle speed N ($N = 60 f_t / n_t = 60 r_t f_n / n_t$) is used instead of r_t. The results in Table 1 are generated using the same data as the example in Tlusty [4]. The parameters are: k = 10, $k_s = 1$, $\zeta = 0.05$, $n_t = 1$, and $f_n = 250$ HZ.

6.4. Properties of the stability lobe diagram

Some interesting characteristics exist in the stability lobe diagram, which may be utilized to optimize the chip width or depth of cut and obtain the maximum material removal rate (MRR) in machining processes.

6.4.1 Stability criteria and chatter lines

In a stability lobe diagram, a series of scallop-shaped lobes intersect with each other. These lobes form the limits for chattering. Locally, for each lobe, it is stable below the lobe, and unstable above the lobe. Since the lobes intersect, a point located below one lobe could be above the neighboring lobe. This point must be treated as unstable. Therefore, globally, we must consider the relationship between adjacent lobes in determining stability. The upper portions of any two adjacent lobes above their intersection point should be trimmed off. The intersection points connect all the lobes into "chained" chatter lines (Figure 6.1.) All the points above the chatter lines are unstable, and below are stable. As spindle speed increases, the lobes become wider with larger intervening spaces between consecutive lobes, and intersection points are higher. This phenomenon creates a desirable situation for machining at both higher speed and deeper cut simultaneously, as well as at a wider speed range.

The two sides of the series of lobes have some special characteristics. The first lobe #0 on the right of the diagram has the maximum stable chip width at its intersection with lobe #1. The right branch of lobe #0 has no intersection with other lobes, which allows unlimited chip width at extremely high spindle speed. Due to the limits of cutter material composition and available motor power, we may not be able to reach the range practically. However, further investigation is needed to verify its theoretical validity. The lobes on the left of the diagram are crowded both horizontally and vertically. The lobes not only become closer together toward the left, but their intersection points also move downward, closer to the minimum chip width (or $r_b = 1$).

However, in real machining processes, bigger chip widths or deeper cuts have been reached without chattering. To solve this problem, Tobias and Fishwick [2] derived a different equation that produces a chatter line with bigger chip width.

6.4.2 The stability regions and their border lines

The entire range of the stability lobe diagram may be divided by the lower and upper border lines (the dashed lines on Figure6.1 and Figure 6.2) into three regions of stability: unconditionally stable, conditionally stable, and unconditionally unstable. The lowest points on the lobes are the minimum chip widths with the same values $(b = b_{\min} at\ r_b = 1)$. A horizontal border line can be formed by connecting the lowest points on the lobes or simply drawn at $b = b_{\min}$. The region below this line is unconditionally stable, which is independent of chatter frequency or spindle speed. We may also fit a curve through or simply connect all intersection points of the lobes to form another border line. The region above this upper border line is unconditionally unstable, and chatter always occurs in the region. The region in between the two regions is conditionally stable. In the conditionally stable region, points are stable when they are below the lobes, and unstable above the lobes. The upper and lower border lines converge to a point of minimum chip width at $r_b = 1$ when the spindle speed approaches zero.

The division into three stability regions with the two border lines provides a distinctive separation between stable and unstable zones. This enables a quick estimate and selection of the allowable chip width for a machining process to prevent chattering, instead of fine tuning the optimum chip width in the conditionally stable region. We can always safely control the cutting in the unconditionally stable region at all ranges of speeds by limiting the chip width to be smaller than $b_{\min}$. Doing so may not utilize the maximum chip width for the MRR, but the quick selection and guarantee of stability are still valuable in applications, especially in small machine shops. The upper border line can also provide a quick check for instability, so that we can avoid the cuttings where chip width falls into the unconditionally unstable region.

6.4.3 The optimum chip width at sweet spots

All lobes intersect with other lobes on both sides, except for the #0 lobe which has no intersection point with other lobes on its right side. The intersection points are the peak points of the lobes, and they provide the deepest cuts at various speed ranges nearby. Therefore, these peak points are called the sweet spots. If we could locate these sweet spots or the optimum depths of cut, we will be able to fully utilize the potential of the machining system and obtain the most efficient material removal rate (MRR). A method is introduced here to analytically determine the approximate sweet spots at the intersections.

The sweetest spot is the intersection of the #0 lobe and #1 lobe, which provides the deepest cut at the highest spindle speed. Due to many other factors, such as the limits of machine power and spindle speed, it may not be practical to operate a specific machine to cut certain workpiece materials at the sweetest spot.

6.5. The optimum chip widths

6.5.1 Difficulties in determining the optimum chip widths

In the past, the optimum chip widths or sweet spots were approximately interpolated read by eye from the stability lobe diagram at the intersections of the lobes. This graphical solution neither utilizes available modern computing power nor provides accurate and consistent numerical values.

Researchers have made efforts to calculate the optimum chip widths. Based on the resonance of frequencies, Smith and Tlusty [6] suggested that the maximum chip widths occur when the tooth frequency f_t (or a multiple of tooth frequencies) matches the natural frequency f_n,

$$f_n = (n+1) f_t \qquad or \qquad r_t = f_t / f_n = 1/(n+1), \qquad n = 0,1,2... \tag{6.11}$$

where the maximum chip width occurs at the intersection of the nth lobe and the $(n+1)^{th}$ lobe. Equation (6. 11) gives results of $r_t = f_t / f_n = 1,1/2,1/3...$ for the consecutive series of

lobes. From the stability lobe diagram (Figure 2), these values on the x-axis correspond to the vertical asymptotes at the left branches of the lobes. At these points, the chip widths are infinite. Smith & Tlusty [6] also made an attempt to relate the chatter frequency f to the tooth frequency f_t. They suggested that the peak point between the n^{th} lobe and the $(n+1)^{th}$ lobe may be found by the intersection of two functions. One of them is the chatter frequency function f for the n^{th} lobe, and the other is the tooth frequency function $(n+1)f_t$, both as function of the tooth frequency f_t (Figure 6.3). The tooth frequency function $(n+1)f_t$ is a simple linear function with expressions of $f_t, 2f_t, 3f_t \ldots$ for the lobes #0, #1, #2, etc. At the intersection points of the two functions, we have

$$f = (n+1)f_t \qquad or \qquad r = (n+1)r_t, \qquad n = 0,1,2... \tag{6.12}$$

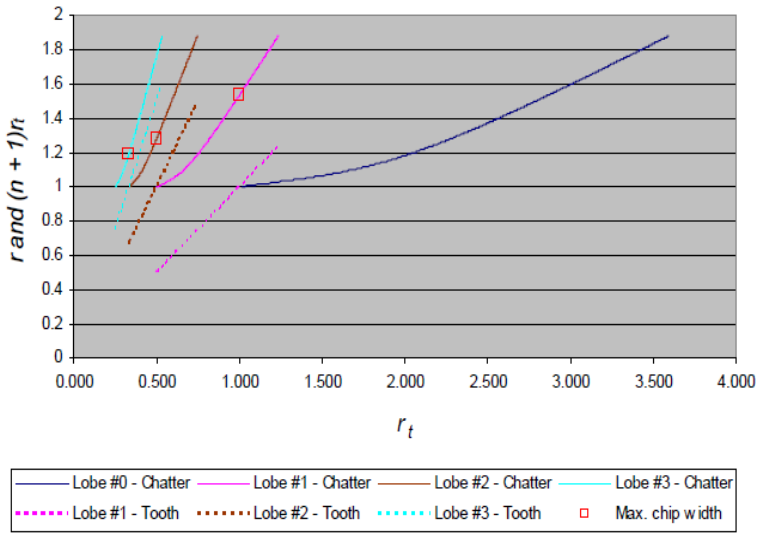

Figure 6.3 Approximate locations of the optimum chip widths

This approach does not work either. Comparing Figure 6.3 with Figure 6.2, we see these intersection points also correspond to the vertical asymptotes at the left branches of the lobes, resulting in infinite chip widths.

Why do both approaches encounter the same difficulty of yielding infinite chip widths? The cause may be the attempt to relate the three frequencies: chatter frequency f , natural frequency f_n , and tooth frequency f_t through equation (6.7, 6.11, and 6.12).

Letting ε = 2π in equation (6.7) produces equation (6.12). However, when ε = 2π, there is no phase shift between the chatter frequency f and tooth frequency f_t . This means that the chatter frequency is equal to the tooth frequency by a factor of (n + 1). When this happens, the two frequencies are in harmony. This situation violates the fundamental assumption of regenerative chatter theory: the chatter is caused by the phase shift between the surface waviness of consecutive cuts.

If we let ε = 0 and $f = f_n$ in equation (6.7), we obtain equation (6.11). Not only is zero phase shift (ε = 0) is not allowed by the regenerative chatter theory, but also the chatter frequency f cannot be equal to the natural frequency f_n . The point at $r = f / f_n = 1$ is a singular point, which makes the real FRF $G_r = 0$ (equation 6.4), and as a result, b = ∞ (equation6.3). This condition results in the vertical asymptotes at the left branches of the lobes.

6.5.2 Approximate solution of the optimum chip widths

Thus far, we have not been able to solve for the intersection points of the lobes. A method is introduced here to analytically calculate the approximate optimum chip widths. It also provides a procedure of finding the sweet spots using a spreadsheet.

Let us look again at the relationship between the chatter frequency f and the tooth frequency f_t ($or\, r = f / f_n \;and\; r_t = f_t / f_n$) . We know from equation (6.11) that when $r_t = 1, 1/2, 1/3...$ the vertical asymptotes exist at the left branches of the lobes in the stability lobe diagrams. At these locations, the chip widths are infinite. However, we may still use the relationship to analytically locate the approximate peak values of the chip

widths or the intersections of the lobes. Figure 6.4 shows both relationships of $r \sim r_t$ and $(n+1)r_t \sim r_t$. At each value of $(n+1)r_t$ on the x-axis, there are two corresponding values of $r, r_n \; and \; r_{n+1}$ r, on the y-axis for any pair of adjacent lobes n and (n + 1). The values of r_n from the n^{th} lobe approach 1, which yields $r_b = \infty$, therefore, not applicable. However, the value of r_{n+1} from the next $(n+1)^{th}$ lobe is finite, which may be used to determine the intersection points of the n^{th} and $(n+1)^{th}$ lobes, i.e., the optimum depths of cut b (or r_b), with very close approximations. These points are marked in Figure 6.3 as squares on the $r \sim r_t$ plots.

The idea of calculating the approximate optimum chip width is actually quite simple. Since the suggested intersection points (equation 6.11 and 6.12) are invalid with infinite chip widths for the n^{th} lobe, we will use the same value on the x-axis to calculate the chip width for the $(n+1)^{th}$ lobe, and obtain the result as an approximate intersection point for the nth and $(n+1)^{th}$ lobes, The governing equations and detailed procedures to calculate the intersection points are as follows.

The approximate intersection point for the n^{th} lobe and $(n+1)^{th}$ lobe is located at the point on the x-axis:

$$r_t = \frac{1}{n+1}, \qquad n = 0,1,2,.... \tag{6.13}$$

For the $(n+1)^{th}$ lobe, from equation (6. 9), we have

$$r^t = \frac{r}{n+1+\frac{1}{2}+\frac{1}{\pi}\tan^{-1}\frac{-2\zeta r}{1-r^2}}, \qquad n = 0,1,2,... \tag{6.14}$$

Substituting equation (6. 13) into equation (6. 14), we obtain

$$\frac{r}{n+1+\frac{1}{2}+\frac{1}{\pi}\tan^{-1}\frac{-2\zeta r}{1-r^2}} = \frac{1}{n+1} \qquad n = 0,1,2,... \tag{6.15}$$

Solve equation (6.15) for r. Substituting r into equation (6.6), we obtain the approximate optimum chip width b (or r_b).

It may require multiple iterations to solve equation (6.15) numerically. It is convenient to use a spreadsheet to calculate the approximate optimum chip width r_b (Table6.2). A step-by-step procedure of the calculations is illustrated in Table (6.2) as an example. In order to compare the results, the same data [4] used to create Figure 6.1 are used here again. The chip width value for each n is the approximate intersection point between the n^{th} lobe and $(n+1)^{th}$ lobe. Both the dimensionless relationship of $r_t \sim r_b$ and the dimensional relationship $N \sim b$ are listed in the table for comparison.

n	r_t	r	r_b	N	b
0	1.000	1.536	6.555	15,002	6.883
1	0.500	1.282	3.186	7,504	3.345
2	0.333	1.195	2.197	4,998	2.307
…	…	…	…	…	…

Table 6.2 Calculated optimum chip widths

Step 1. For lobe number n, calculate r_t from equation (6. 13).

Step 2. Also for lobe number n, calculate r by iteration from equation (6.15).

Step 3. Substitute r into equation (6. 9) to obtain r_b.

Step4.The result of r_b is the approximate optimum chip widths at r_t for the intersection of the n^{th} and $(n+1)^{th}$ lobes. The results may also be written as the spindle speed vs. chip width $N \sim b$.

The calculated approximate analytical solutions of the intersections (Table 6.2) are plotted in Figure 6.2, and marked by square symbols. The intersection values interpolated by graphic solutions (also approximate) from Figure 6.1 are also listed in Tale 6.3 for comparison with the approximate analytical solutions in Table 6.2. From Figure 6.2 and the comparison of the data in Table 6.2 and Table 6.3, the calculated approximate points are located to the left of the "actual" intersections. The differences of the optimum chip

widths (b *or* r_b) between the analytical calculations (Table 6.2) and the interpolated graphic solutions (Table 6.3) are closer in absolute values toward lower spindle speeds, while smaller in relative variations toward higher spindle speeds. At the sweetest spot or the intersection of the #0 lobe and #1 lobe, the difference of r_b is 0.575 or 8%. Therefore, the method can be used to analytically calculate a good approximation of optimum chip widths for MRR.

n	r_t	r	r_b	N	b
0	1.027	1.536	7.130	15,404	7.487
1	0.515	1.282	3.598	7,721	3.778
2	0.344	1.195	2.583	5,161	2.712
…	…	…	…	…	…

Table 6. 3 Graphic solutions of optimum chip widths

6.6. Application of Segmented Beam Formulation

The determination of fundamental natural frequency for segmented beam is explained in chapter 5. Because of the complex matrix calculations (equation 5. 35), the determination of natural frequency is very difficult. Therefore, a graph was created based on the geometric properties of the beam. From this graph (Figure5.3) K value can be selected to calculate natural frequency. Then, simplified equations were developed according to length ratio (L1/L2) and diameter ratio (D1/D2) (equation 5.40). Fundamental natural frequency can be easily calculated by using K value, geometric properties and material properties (equation 5.39).

For this section, two segmented beams, which have different materials and geometric properties, are selected (Figure 6.4). In this analysis, the length and diameter ratios are more important than the exact length diameter values. The mechanical properties of the material are given in Table 6.4 [Beer and Johnston, 1992]

Figure 6.4: Geometric properties of aluminum and steel segmented beams

MATERIAL	Elastic modulus(GPa)	Density(kg/m^3)
steel	200	7860
Aluminum	72	2800

Table 6.4: Mechanical properties of the segmented beam materials

The K value is calculated from the matrix solution (equation 5.35), the graph (Figure 5.3) and the simplified equations (equation 5.40). Following calculation shows the K value determination from simplified equations for aluminum segmented beam. Table 6.5 shows all K values for three different methods.

$$\frac{1}{K} = a\left(\frac{D1}{D2}\right) + b \rightarrow K = \frac{1}{a\left(\frac{D1}{D2}\right) + b} \qquad \text{and} \qquad a = \frac{-0.817(\ln l) + 0.0167}{l}$$

$$b = 0.1821l^2 + 0.1063l - 0.0275$$

$$l = \frac{L1}{L2}$$

$$l = \frac{L1}{L2} = 0.57, \qquad \frac{D1}{D2} = 1.45 \quad \rightarrow K = 0.767$$

K	MATRIX	GRAPH	EQUATION
L1/L2=0.57,D1/D2=1.45 Aluminum	0.808	0.790	0.767
L1/L2=0.31,D1/D2=1.25 Steel	0.271	0.260	0.253

Table 6.5: K values for three different methods of natural frequency calculation

Material properties, geometric properties and K values for all methods are substituted into equation 5.39 and natural frequency is calculated. Following calculation demonstrates natural frequency of the aluminum segmented beam.

$$\omega_{matrix} = \frac{0.808}{2\pi}\sqrt{\frac{72.10^9 \frac{\pi(0.029)^4}{64}}{2800\frac{\pi(0.029)^2}{4}(0.130)^4}} = 279Hz$$

$$\omega_{graph} = \frac{0.790}{2\pi}\sqrt{\frac{72.10^9 \frac{\pi(0.029)^4}{64}}{2800\frac{\pi(0.029)^2}{4}(0.130)^4}} = 273Hz$$

$$\omega_{equation} = \frac{0.767}{2\pi}\sqrt{\frac{72.10^9 \frac{\pi(0.029)^4}{64}}{2800\frac{\pi(0.029)^2}{4}(0.130)^4}} = 265Hz$$

FREQUENCY(Hz)	MATRIX	GRAPH	EQUATION
L1/L2=0.57,D1/D2=1.45 Aluminum	279	273	265
L1/L2=0.31,D1/D2=1.25 Steel	671	651	621

Table 6.6: Frequency results for three different methods

After determining the natural frequency, the mode shape can be obtained by using arbitrary constant vector A from equation (5.34). The mode shape, which is obtained by using the solution for matrix equations for aluminum beam, is given in Figure 6.5.

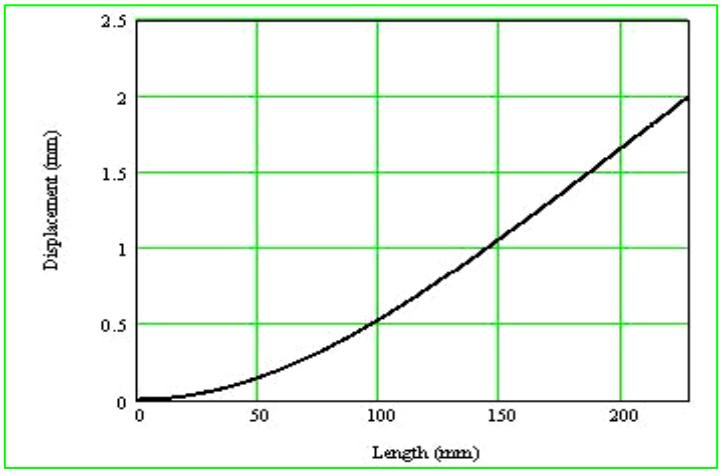

Figure 6.5: Mode shape for the solution of matrix equations

For the first bending mode, maximum displacement occurs at the end of the beam. The comparison of the mode shapes of the aluminum segmented beam for all three methods is given in Table 6.7. The table contains the ratio of displacement at certain point and maximum displacement.

Displacement/ Max Displacement	at 50 mm	at 100 mm	at 150 mm	at 200 mm	at 228 mm
MATRIX	0.07325	0.26597	0.53145	0.82955	1
GRAPH	0.07579	0.27009	0.53515	0.83095	1
EQUATION	0.07896	0.27526	0.53975	0.8327	1

Table 6.7: The comparison of the mode shapes for three different methods

6.7 Summery

In this chapter, an analytical method is presented here to calculate the approximate optimum chip widths. A step-by-step procedure for doing the calculation using a spreadsheet is also presented. The intersections or sweet spots of the consecutive series of lobes provide the optimum chip widths. In the past, the sweet spots were found by graphic solutions from the stability lobe diagram The results of the method show that they are close to the actual values, especially for the sweetest spot at the intersection of the #0 lobe and #1 lobe, which provides the stable machining at the highest spindle speed and the deepest depth of cut. The method may be used to easily obtain a quick estimate of the optimum chip widths for calibrating the cutting parameters and the figures and tables were created using the same data as the example by Tlusty [4] for verifications of the methods and comparisons of results. Finally, the application of the simplified segmented beam equations is demonstrated with examples.

CHAPTER SEVEN
CONCLUSION

In this study, generalized equations are presented which can be used for predicting the static and dynamic properties of end mill. Both FEA and analytical methods have been used for static and dynamic analysis. The models consider the complex geometry of flutes in development of cross sectional properties. And also, geometric properties and material characteristics of tool and tool holder are explained. Models for end mill static deformations, which can be used for deflection calculations and surface form error, are presented. The static characteristics of tool and tool holder are obtained using FEA analysis. FEA results are compared with analytical equation results.

End mills have flutes and unfluted sections, which further complicate their geometry. This segmented characteristic has also been considered in static and dynamic modeling. This is an original contribution of this work. Simplified equations for segmented beam can be used for any area. Therefore, simplified equations are created to predict deflections of tools for given geometric parameters and material properties. Due to its wide use in industry, milling process is considered, however the same methods can be applied to other machining operations as well.

A method of modeling for transverse vibrations of geometrically segmented beam is proposed. End mill is assumed to be as segmented beam with one end fixed and other end free. In order to obtain natural frequency and mode shape of the system, complex matrix calculations are needed. Simplified equations are derived to eliminate time consuming calculations. In these equations, desired geometric properties can be selected for prediction.

Finite Element Analysis (FEA) results of various tool geometries, different materials and tool holder types are given. These results are compared with the results obtained from analytic equations.

A method of using a spreadsheet to create stability lobe diagrams is presented. This step-by-step procedure provides an easy way for machine operators to choose the optimum chip widths and high spindle speeds at the sweet spots on the diagram to obtain a high material removal rate (MRR). It also helps students to understand the theory of machine chattering, and practice on the optimum cutting parameters in machining processes. A stability lobe diagram is composed of a series of scallop-shaped chatter lines. It may be represented either as the relationship between the chip width or depth of cut and spindle speed as b ~ N, or as a dimensionless relationship between the ratios of the chip width to the minimum chip width and the tooth-stroke frequency to the natural frequency as r_b and r_t. The dimensionless relationship is preferable because it makes it easy to compare machining processes under different cutting parameters and conditions.

As a future work Frequency Response Function (FRF) measurements need to be performed to identify the dynamics of the system experimentally. The FRFs using analytical models and the receptance coupling substructure analysis (RCSA) can be compared with experimental results for verification. For the identification of the interface stiffness and damping between the tool and tool holder, different tool geometries, materials and clamping conditions can used. Contact parameters will identify and present. The modeling of contact parameters will be developed. The parameters can be determined by using these models according to tool geometric conditions, material properties and clamping force. In the future, all study, which is done for tool and tool holder, can be done for spindle and machine. All models can be integrated into CAD/CAM systems to develop a virtual machining system for precision machining.

Machining is a very complicated process. There are many parameters that contribute to the interactions between machine tool, cutting tool, and workpiece. More complications also arise in multiple degrees of freedom in multi-mode machine chattering. Due to the limit of the scope, we have only discussed the fundamental concepts and procedures in creating a stability lobe diagram. More discussion of the regenerative chatter theory and the stability lobe diagram can be presented as a future work.

REFERENCES

1. Beer, F., Johnston, E., 1992, Mechanics of Materials, Mcgraw-Hill , U.K.

2. Budak, E., 1994, The Mechanics and Dynamics of Milling Thin-Walled Structures, Ph.D. Dissertation, University of British Columbia.

3. Budak, E. and Altintas, Y., 1994, Identification of Peripheral Milling Conditions for Improved Dimensional Accuracy, Int.J. Machine Tools and Manufacture, 34/ 7:907-918.

4. Budak, E. and Altintas, Y., 1995, Modeling and avoidance of static deformations in peripheral milling of plates. International Journal of Machine Tools and Manufacture, 34/ 3:459-476.

5. Budak, E., Altintas, Y. and Armarego, E.J.A., 1996, Prediction of Milling Force Coefficients From Orthogonal Cutting Data, Trans. ASME Journal of Manufacturing Science and Engineering, 118:216-224.

6. Altintas, Y. and Lee, P., 1996, A general mechanics and dynamics model for helical end mills. Annals of the CIRP, 45: 59-64.

7. Altintas, Y. and Engin, S., 2001, Generalized modeling of mechanics and dynamics of milling cutters, Annals of the CIRP, 50: 25-30.

8. Budak, E. and Altintas, Y., 1998, Analytical prediction of chatter stability in milling-Part I: General formulation; Part II: Application to common milling systems. Trans. ASME, Journal of Dynamic Systems, Measurement, and Control, 120:22-36.

9. Shih, R., 2000, Introduction to Finite Element Analysis, SDC

10. Budak, E., 2002, Modeling End Milling Process Including Part-Tool Flexibility and Dynamics", Proceedings of 3rd International Seminar on Intelligent Computation in Manufacturing Engineering (ICME 2002), 243-250, Ischia, Italy.

11. Kivanc, E., Budak, E., 2003, Proceeding of Modelling Statics and Dynamics of Milling System Components, Proceedings of the CIRP International Seminar on Manufacturing Systems, Saarbrucken, Germany.

12. Kline, W.A., DeVor, R.E., and Shareef, I.A., 1982, The prediction of surface accuracy in end milling. Trans ASME Journal of Engineering for Industry, 104: 272-278.

13. Koenigsberger, F. and Sabberwal, A.J.P., 1961, An investigation into the cutting force pulsations during milling operations. International Journal of Machine Tool Design and Research, 1:15-33.

14. Koenigsberger, F. and Tlusty, J., 1967, Machine Tool Structures-Vol. I: Stability Against Chatter, Pergamon Press.

15. Kops, L. and Vo, D., 1990, Determination of the Equivalent Diameter of an End Mill Based on Its Compliance, Annals of the CIRP, 39:93-96.

16. Smith, S. and Tlusty, J., 1991, An overview of modeling and simulation of the milling process. Trans. ASME Journal of Engineering for Industry, 13:169-175

17. Tlusty, J. Machine Dynamics. Handbook of High Speed Machining Technology. King, R.I., ed., 1985, Chapman and Hall, New Tork, Ch. 3, 48-153.

18. Tlusty, J. Dynamics of high-speed milling. J. of Engineering for Industry, Trans. ASME, 108, May 1986, 59-67.

19. Budak, E. & Altintas, Y. Analytical prediction of chatter stability in milling-Part II:

Application of the general formulation to common milling systems. J. Dynamic Systems, Measurement, and Control, Trans. ASME, 120, 1998, 31-36.

20. Altintas, Y., Shamoto, E., Lee, P., & Budak, E. Analytical prediction of stability lobes in ball end milling. J. Manufacturing Science & Engineering, Trans. ASME, 121(4), 1999, 586-592.

21. Smith, S. & Tlusty, J. Update on high-speed milling dynamics. J. Engineering for Industry, Trans. ASME, 112, May 1990, 142-149.

22. Altintas, Y. & Budak, E. Analytical prediction of stability lobes in milling. Ann. CIRP, 44(1), 1995, 357-362.

23. Minis, I. & Yanushevsky, R. A new theoretical approach for prediction of stability lobes in milling. ASME J. Eng. For Ind., 115, Feb. 1993, 1-8.

24. Jemielniak, K. & Widota, A. Suppression of self excited vibration by the spindle speed variation method. Int. J. Mach. Tool. Des. Res., 24(3), 1994, 207-214.

25. Jayaram, S., Kapoor, S. G., & DeVor, R. E. Analytical stability analysis of variable spindle speed machining. J. Manufacturing Science & Engineering, Trans. ASME, 122, Aug. 2000, 391-397

26. Engin, S. and Altintas, Y. Mechanics and dynamics of general milling cutters, Part I: Helical end mills. Int. J. Mach. Tools Manuf., 41(15), 2001, 2195-2212.

27. Fofana, M. S. Aspects of stable and unstable machining by Hopf bifurcation. Applied Mathematical Modelling, 26(10), October 2002, 953-973.

28. Fofana, M. S. Sufficient conditions for the stability of single and multiple regenerative chatter. Chaos, Solitons and Fractals, 14, 2002, 335-347.